JOURNAL OF GEOPHYSICAL RESEARCH, VOL. 106, NO. C1, PAGES 879–897, JANUARY 15, 2001

Remote forcing at the Last Glacial Maximum in the Tropical Pacific Ocean

Dyke H. Andreasen

Earth Sciences Department, University of California, Santa Cruz, California

A. Christina Ravelo

Institute of Marine Sciences, University of California, Santa Cruz, California

Anthony J. Broccoli

Geophysical Fluid Dynamics Laboratory, Princeton University, Princeton, New Jersey

Abstract. We present results of a Last Glacial Maximum (LGM) wind stress sensitivity experiment using a high-resolution ocean general circulation model of the tropical Pacific Ocean. LGM wind stress, used to drive the ocean model, was generated using an atmospheric general circulation model simulation forced by LGM boundary conditions as part of the Paleoclimate Modeling Intercomparison Project (PMIP) [*Broccoli*, 2000]. LGM wind stress anomalies were large in the western half of the basin, yet there was a significant hydrographic response in the eastern half. This ocean model experiment hind casts changes that are in close agreement with paleoceanographic data from the entire region, even without the explicit modeling of the air-sea interactions. Data and model both predict that the annual average thermocline tilt across the basin was enhanced. Data and model are consistent with a stronger equatorial undercurrent which shoaled to the west of where it does today, and stronger advection of water from the Peru Current into the east equatorial Pacific and across the equator. Paleoproductivity and sea surface temperature (SST) data are interpreted in light of the modeling results, indicating that paleoproductivity changes were related to wind-forced dynamical changes resulting from LGM boundary conditions, while SST changes were related to independent, possibly radiative, forcing. Overall, our results imply that much of the dynamic response of the tropical Pacific during the LGM can be explained by wind field changes resulting from global LGM boundary conditions.

1. Introduction

Continuity requires the loss by advection of wind-driven surface waters to the western tropical Pacific be, in part, compensated in the eastern equatorial Pacific (EEP) by upwelling and replenishment via the nutrient-enriched equatorial undercurrent. One ramification of this dynamic is that roughly 25-50% of modern day global "new" production via phytoplankton growth could occur in the EEP [*Chavez and Barber*, 1987]. On geologic timescales, variation of the trade wind-driven circulation may be of fundamental importance to the regulation of greenhouse gases and/or global ocean nutrient levels (through denitrification in the EEP) [*Tans et al.*, 1990; *Toggweiler et al.*, 1991; *Toggweiler and Carson*, 1995; *Ganeshram et al.*, 1995; *Sarnthein et al.*, 1988]. Higher productivity of Last Glacial Maximum (LGM, 20,000 years ago) tropical Pacific waters along the equator and particularly in the EEP is well documented [e.g., *Pedersen*, 1983; *Lyle et al.*, 1988, *Lyle*, 1988; *Pedersen et al.*, 1988, *Pedersen*, 1991; *Sarnthein et al.*, 1988; *Paytan et al.*, 1996]. There have been suggestions that this enhanced productivity (and lower sea surface temperatures (SST)) is directly related to enhanced wind-driven divergent upwelling [*Arrhenius*, 1952, 1988; *Moore et al.*, 1980; *Climate: Long-Range Investigation, Mapping, and Prediction (CLIMAP) Project Members*, 1976, 1981; *Lyle et al.*, 1992; *Murray et al.*, 1993]. This seems to be supported by a steeper than modern E-W tilting thermocline [*Andreasen and Ravelo*, 1997; *Patrick and Thunell*, 1997] which lead to the canonical view that enhanced southeast trades and Walker circulation existed at the

Paper number 1999JC000087
0148-0227/01/1999JC000087$09.00

LGM. Enhanced Walker circulation should have been accompanied by a stronger zonal SST gradient, but there is still considerable controversy regarding tropical SSTs [e.g., *CLIMAP*, 1976, 1981; *Rind and Peteet*, 1985; *Guilderson et al.*, 1994; *Bush and Philander*, 1998]. Therefore, the conclusion that enhanced EEP paleoproductivity in the LGM is a result of stronger Walker circulation which forced stronger divergent upwelling is circumstantial. In addition, phase differences between SST and productivity proxies, which we will detail below, and their direct relationship to local winds are not clear cut.

In this study we synthesize and reconcile known changes in hydrography, productivity, and wind patterns in the tropical Pacific to understand conditions during a glacial extreme (the LGM). Our study uses winds predicted by an atmospheric general circulation model (AGCM) simulation of the LGM to investigate hydrographic sensitivity to those winds applied to a high-resolution ocean general circulation model. Our approach is to use LGM observations of thermocline depth changes which are very sensitive to wind stress changes to evaluate our model results. This model-data comparison aims to put observations of conditions during the LGM into an oceanographically consistent basin-wide framework.

2. Background

Tropical Pacific thermocline depth structure arises due to a westward surface pressure force which is maintained by persistent easterly trade winds. At a depth of ~200 m the water column depth integrated pressure gradient compensates for the westward intensifying surface pressure gradient and results in a westward deepening thermocline [*Meyers*, 1979] (Figure 1). Variations in the zonal pressure gradient in the western Pacific drive intraannual equatorial thermocline depth variability at 140°W, whose maximum range is roughly 50 m[*Levitus and Boyer*, 1994]. Furthermore, variability at 140°W is correlated to winds at 165°E but is uncorrelated with local winds [*Murray et al.*, 1994]. Interannual thermocline excursions can exceed 180 m at 140°W and much like the La Niña mode today, a steeper E-W thermocline tilt is estimated for the LGM [*McPhaden and Hayes*, 1990; *Andreasen and Ravelo*, 1997]. However, intraannual variability involves tropical dynamics whose timescales are too short to serve as analogs to LGM thermocline depth excursions, and intensified trade winds of a La Niña involve strong intratropical air-sea feedbacks and internal ocean dynamics whose tropical cause may be very different from those of global LGM forcing factors.

The equatorial undercurrent (EUC) flows eastward confined in a narrow band (2°N to 2°S) roughly within the main thermocline bounded by 24 and 26 kg m^{-3} isopycnals [*Wyrtki and Kilonsky*, 1984]. This conduit serves as an important source of trace elements to the EEP and as a source of nutrients both from within the EUC core and via entrainment of nutrient rich deeper EUC waters into the mixed layer [*Barber and Chavez*, 1991; *Coale et al.*, 1996a; *Toggweiler and Carson*, 1995; *Guilderson and Schrag*, 1998; *Wyrtki*, 1981]. Given the importance of the undercurrent in greenhouse gas regulation and productivity, variations in EUC transport, sources, or nutrient content either within its core or off of Peru, could have substantial ramifications on the Central Equatorial Pacific (CEP) and EEP sedimentary record.

Debate exists about the relative roles of local and remote wind stress forcing on the zonal momentum balance in governing EUC variability observed in the central Pacific (~140°W) [*Philander and Pacanowski*, 1980; *McPhaden and Taft*, 1988; *Philander and Chao*, 1991; *Yu et al.*, 1997; *Wacongne*, 1989, 1990]. In terms of local zonal winds, many studies have investigated the relative importance of linear (vertical mixing) versus nonlinear (vertical advection) terms of the momentum balance equation (at 140°W) in modulating the intraannual eastward momentum of the EUC [e.g., *Philander and Pacanowski*, 1980; *Halpern*, 1980; *Knauss*, 1966;

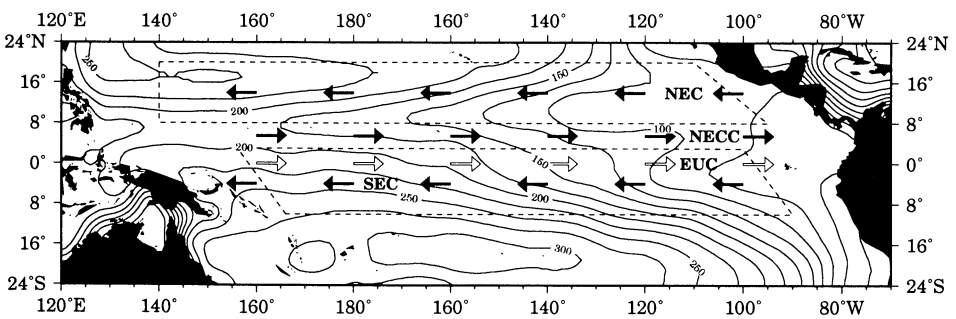

Figure 1. Contour plot of annual average thermocline (18°C isotherm) depth (in meters) in the tropical Pacific. Thermocline depth is derived from the world ocean atlas of *Levitus and Boyer* [1994]. Arrows show the circulation of the four major Tropical Pacific Ocean currents: the South Equatorial Current (SEC), the North Equatorial Current (NEC), the North Equatorial Countercurrent (NECC), and the Equatorial Undercurrent (EUC). Dashed lines show the latitudes which bound the easterly flowing currents.

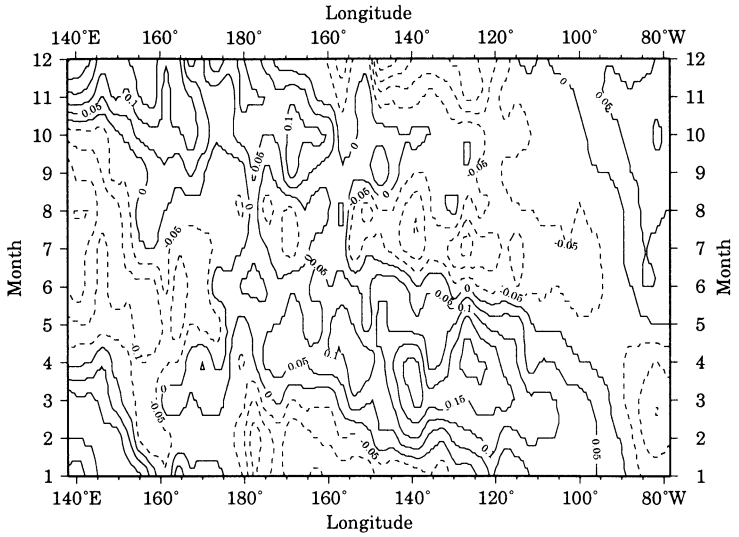

Figure 2. Zonal wind stress anomaly (i.e., monthly wind stress departure from the annual mean) equatorial transect in the Pacific Ocean show the westward propagation and the out of phase relationships between winds in the east and west [*Meyers*, 1979; *Philander and Chao*, 1991; *Yu et al.*, 1997]. Positive (negative) values indicate wind stress was anomalously westerly (easterly) (climatological wind stress from *Hellerman and Rosenstein*, [1983]).

McPhaden and Hayes, 1990; *Yu et al.*, 1997]. In terms of remote effects it has been proposed that the advection of eastward subsurface momentum is nearly balanced by the zonal pressure gradient in the western equatorial Pacific. Across the equatorial Pacific, wind anomalies are not uniform but partitioned within meridional westward propagating bands (Figure 2) [*Meyers*, 1979; *Lukas and Firing*, 1985]. Thus in the boreal spring when the undercurrent is maximal, a westerly wind anomaly in the east can be out of phase with a coeval easterly anomaly west of 140°W [*Philander and Chao*, 1991]. By the latter half of the year, anomalous easterlies prevail in the east-central Pacific, while anomalous westerlies prevail in the west. Modeling studies have attributed the acceleration of undercurrent and its springtime intensification to the large fetch in the western equatorial Pacific [*Philander and Chao*, 1991]. Despite a lack of consensus about whether local linear processes in the central Pacific or zonal extent and magnitude of the pressure force of winds further west are dominant in determining undercurrent speed, both processes appear important.

3. Model Description and Experiment

This study used the Geophysical Fluid Dynamics Laboratory (GFDL) Modular Ocean Model (MOM2) covering the world oceans within 50° of the equator [*Philander and Pacanowski*, 1986a, 1986b]. Spatial resolution for longitude is 1° (100 km at the equator) and 33 km ($\frac{1}{3}$°) for latitude within 10° of the equator, linearly increasing to 100 km by 20° and remains 100 km between 20-50° in both hemispheres. Realistic ocean topography is used except for islands and continental shelves which are set to 300 and 50 m below the sea surface, respectively. The model has 27 levels down to 4919 m, 10 of which are in the upper 100 m of the water column. Heat fluxes at the surface are defined according to *Rosati and Miyakoda* [1988] who use bulk formulas at the ocean surface for determination of surface temperature and salinity. A surface mixing scheme to compensate for higher frequency variability in the wind stress than monthly averages used here was formulated by *Pacanowski and Philander* [1981].

The experimental design involved two simulations. The surface momentum field for the standard model run (SMR) was the *Hellerman and Rosenstein* [1983] mean monthly wind stress monthly climatology (Figure 3a). Monthly surface freshwater fluxes, temperature, and relative humidity came from the Comprehensive Ocean-Atmosphere Data Set [cf. *Slutz et al.*, 1985; *Woodruff et al.*, 1987]. Initially, the model temperature and salinity fields were set to mean January climatology [*Levitus*, 1982] and zero currents. The model was spun up for 4 years at a 40-min time step, and the presented results are from model year 5. Our LGM ocean model run (LGMR) used the wind stress field anomaly predicted by the GFDL coupled atmospheric-mixed layer ocean general circulation model (A-MLO, R30 version) simulation of the LGM [*Broccoli*, 2000] (Figure 3b). The LGM A-MLO simulation is the GFDL contribution to the Paleoclimate Modeling Intercomparison Project (PMIP) which used standardized boundary conditions: (1) atmospheric CO_2 concentrations were reduced by 28% below preanthropogenic levels, (2) LGM reconstructed ice sheet [*Peltier*, 1996], (3) sea level was lowered 105 m, and (4) 21 kyr orbital parameters. A-MLO model calculations of SST are based on the simulated heat fluxes at the air-sea interface [*Broccoli*, 2000]. The

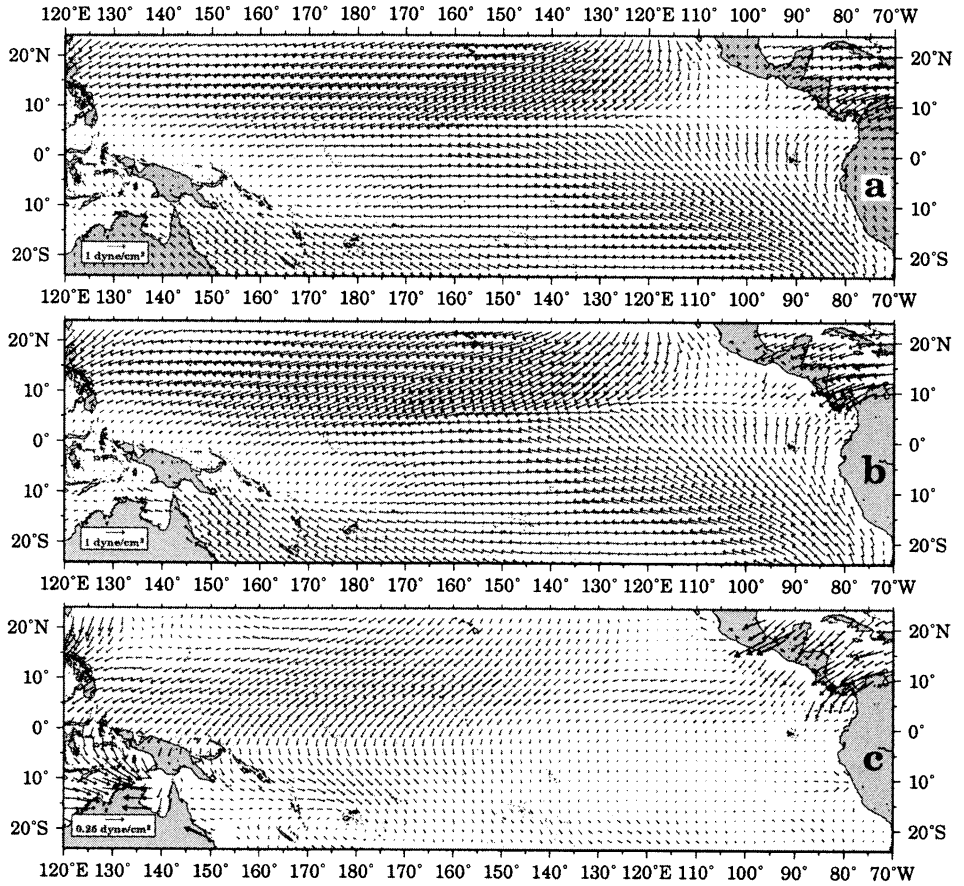

Figure 3. (a) Climatological wind stress [*Hellerman and Rosenstein*, 1983], (b) GFDL atmospheric model wind stress predicted for the LGM, and (c) wind stress anomaly (LGM predicted minus climatological winds).

LGMR was driven by the LGM A-MLO model wind stress anomaly (the difference between the LGM A-MLO model predicted wind stress field minus the A-MLO model standard "present-day" wind stress field) added to the climatological wind stress of *Hellerman and Rosenstein* [1983] (Figure 3c). Thus the only difference between the LGMR and SMR is the added wind anomaly of the LGM A-MLO simulation. All other boundary conditions are the same in both simulations. The LGMR used the spun-up (year 4) SMR as initial conditions and was run for 4 years. Equilibrium of equatorial dynamics for the 4-year integration occurs rapidly (within a year), though dynamics with longer time constants such as tropical-subtropical exchange [e.g., *Liu and Philander*, 1995] have not reached equilibrium. Anomalous SST cooling observed in the LGM experiment (3.5°-4°C in the western warm pool) is an artifact of the ocean model calculations, resulting from a zero relative humidity setting in the heat flux module resulting in a substantial heat loss by evaporation. Despite the anomalous cooling, the model hydrographic response to the perturbed winds remains faithful to those winds and reveals robust, valuable insight into LGM surface ocean sensitivity.

Coupled ocean-atmosphere interactions are integral to tropical Pacific climatology and dynamics and undoubtably remain so at the LGM [*Dijkstra and Neelin*, 2000; *Bush and Philander*, 1998; *Liu et al.*, 2000]. Coupled modeling studies show easterlies spawned via extratropical processes cause the tropical ocean to tend toward cooler SST in the east, but these easterlies are nonlinearly modified in a chain of intrabasin feedbacks involving the trade winds and upper ocean dynamics which affect the E-W SST gradient [*Dijkstra and Neelin*, 1995]. The main results of our uncoupled LGM ocean model simulation reflect extratropical forcing and hence important intrabasin feedbacks and adjustments to this remote forcing are not explicitly modeled. However, our LGM results indicate the spatial structure of the winds, thermocline, and SST gradients in the tropical Pacific Ocean was (slightly) modified by LGM extratropical factors, but in general these patterns are similar to today. This is consistent with the idea that intrabasin coupled feedbacks control the climatology [*Dijkstra and Neelin*, 1995].

General model-data agreement (detailed below) imply the wind field driving the ocean model may be close to accurate. As such, we outline factors in the LGM A-MLO simulation [*Broccoli*, 2000] which are important to changes in the tropics. Two factors of the A-MLO simu-

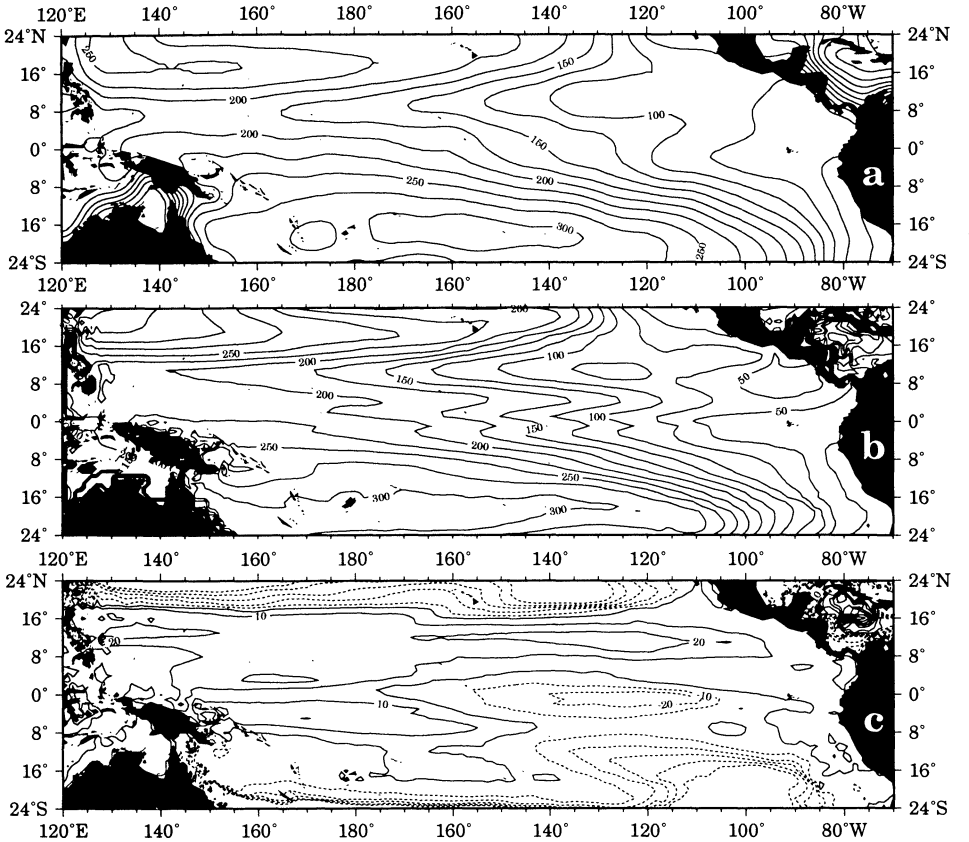

Figure 4. (a) Thermocline (18°C isotherm) depth climatology (derived from *Levitus and Boyer*, [1994]). (b) Standard ocean model predicted thermocline depth (meters). (c) Thermocline depth anomaly (model LGMR-SMR), as reflected in changes in the depth of the 18°C isotherm. For Figure 4c, positive (negative) contours indicate the thermocline depth deepened (shoaled) for the LGM simulation.

lation are responsible for north and western tropical Pacific intensification of LGM winds, relative to the SMR (Figure 3c). First, LGM intensification of northeast trades results from an extratropical cooling asymmetry between hemispheres. Greater extratropical Northern Hemisphere cooling resulted from a radiative inhomogeneity of surface albedo forcing reflecting the presence of large North American and Euroasian continental ice sheets. Second, northeast trade wind intensification was greater in the west, in part because strong SST gradients in the east tend to inhibit Intertropical Convergence Zone (ITCZ) movements relative to weaker SST gradients over the warm pool. In addition, lower sea level resulted in intensified maritime continent convection over exposed land in the Timor Strait-Arafura sea region. Thus the LGM tropical winds calculated using the A-MLO model [*Broccoli*, 2000] and used to drive the OCGM in this study result from both extratropical and tropical conditions.

4. Results

4.1. Standard Model Run

How well does the standard model run (SMR) reproduce observed thermocline (18°C isotherm) depth? In general, smooth thermocline depth contours [*Levitus and Boyer*, 1994] (Figures 1 and 4a) reflect monthly averaging of temperature data from many years, whereas the structure seen in the model simulations (Figure 4b) are more representative of real oceanographic gradients observed in any particular time [see *Ravelo et al.*, 1990]. For thermocline depths shallower than 100 m the model agrees with observation. In regions where the thermocline is deeper than 100 m, the model overestimates thermocline depth by roughly 25 m. One region of notable exceptions is in the northeast tropical Pacific where model estimated thermocline is deeper by >75 m than observation (Figures 4a and 4b). GFDL ocean model mixing parameterizations tend to underestimate thermocline depth [*Richardson and Philander*, 1987], while the wind stress climatology of *Hellerman and Rosenstein* [1983] are overestimated by about 20%-25% in the tropics [*Harrison*, 1989]. However, since we are primarily concerned with anomalies and not absolute values, discrepancies between model and climatology should not bias our interpretations significantly. The SMR resolves modern surface currents well and realistically reproduces conditions in the tropical oceans [*Philander and Pacanowski*, 1986a, 1986b; *Philander et al.*, 1987]. The SMR has maximum EUC speed (>120

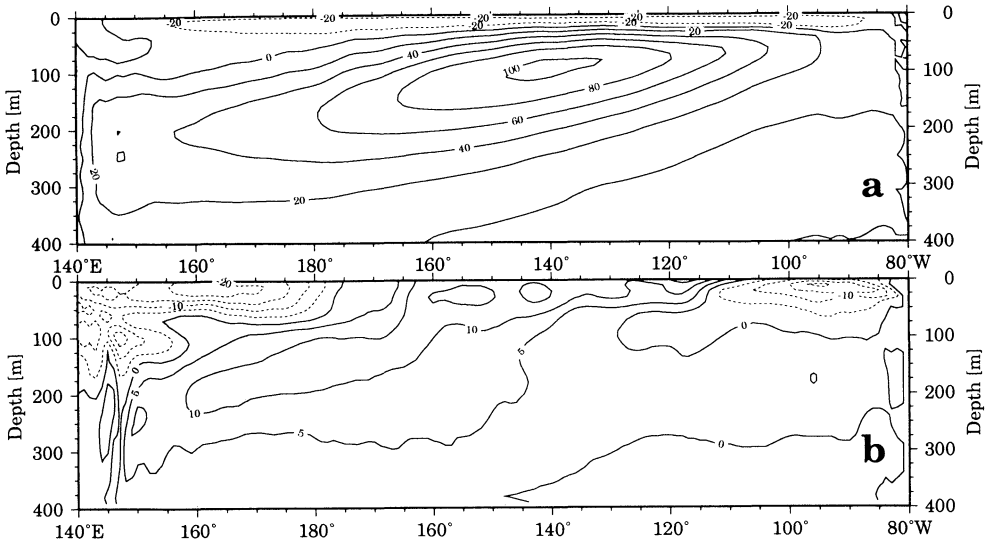

Figure 5. (a) Ocean model results of upper surface ocean (0-400 m) zonal (u) velocity (cm s^{-1}) contour map along the equator. Dashed contours indicate westward flow. (b) Ocean model zonal velocity anomaly map of Last Glacial Maximum run minus the standard model (LGMR-SMR). Note the outcropping and strengthening of the equatorial undercurrent in the central equatorial Pacific and weakening further east.

cm s^{-1}) and transport (45 Sv) in May at 140°W, in reasonable agreement with observation (Figure 5) [*Wyrtki and Kilonsky*, 1984].

4.2. LGM Simulation

4.2.1. Thermocline response. The LGMR demonstrates the response of the thermocline (Figure 4c) to the wind stress anomaly (Figure 3c). LGMR winds at 0.5°N and 5.5°N in the west (165°E) are uniformly and substantially stronger (on average 0.15 dyne cm^{-2}, ≈20%) than modern climatological winds, with the exception of October at 0.5°N (Figures 6c, 6d, 6h and 6i). A stronger local surface pressure gradient over the western Pacific is compensated by an increase in water column depth integrated pressure [*Meyers*, 1979] and results in the western deepening of the thermocline. In the east, along the equator at 105°-155°W, there is a region of substantial thermocline shoaling by as much as 28 m, even though the local wind stress is only slightly stronger during part of the year (Figures 3c and 7). The steepening of the cross-basinal thermocline tilt is most likely due to the higher cross-basinal pressure gradient resulting from the dramatically enhanced easterly winds in the western half of the basin (Figures 3c and 7).

Another notable feature of the LGMR, which will be discussed in more detail in the context of the paleoceanographic observations, is a local wind-driven deep thermocline depth anomaly in the central Pacific along the region of off-equatorial divergence between the North Equatorial Current (NEC) and North Equatorial Countercurrent (NECC) (Figure 4). In addition, east of 100°W the thermocline depth anomaly in the LGMR is small (<10 m), with the exception of the southeast Pacific. In the southeast Pacific the LGMR thermocline depth anomaly is up to about 50 m shallower, roughly centered at 20°S -102°W and extending to the northwest to 10°S and 140°W. However, the model did not reach equilibrium in this region; through the model simulation there was progressive shoaling of the 18°C isotherm by over 100 m at 19°S-110°W as part of a substantial subsurface cooling in this region (see discussion below).

To understand the climate mechanisms responsible for the mean annual conditions described above, it is useful to consider the seasonal hydrographic response to wind forcing in our model simulations. We focus on 140°W, an area of intense physical and biological study in the modern ocean [e.g., *McPhaden and Hayes*, 1990; *Murray et al.*, 1994]. While slightly enhanced local winds (<8% stronger) in the LGMR at 140°W in the early and late part of the year (Figure 6f) are synchronous with local shoaling of the thermocline during those months (Figure 6g), weaker winds in July and August are not accompanied by a discernible thermocline response. Rather, remote wind stress anomalies at 162°E (Figure 6h and 6i) appear to be associated with vertical migrations of the thermocline at 140°W (and the entire CEP). Minima in the LGM wind stress anomaly occurring in July through October (Figures 6h and 6i) correspond (with approximately 1 month lag) to the minimum in the thermocline depth anomaly at 140°W (Figure 6g). This west-to-east connection is due to the eastward propagation of the western thermocline adjustments to LGM wind stress changes. This mechanism also explains the modern seasonal cycle in

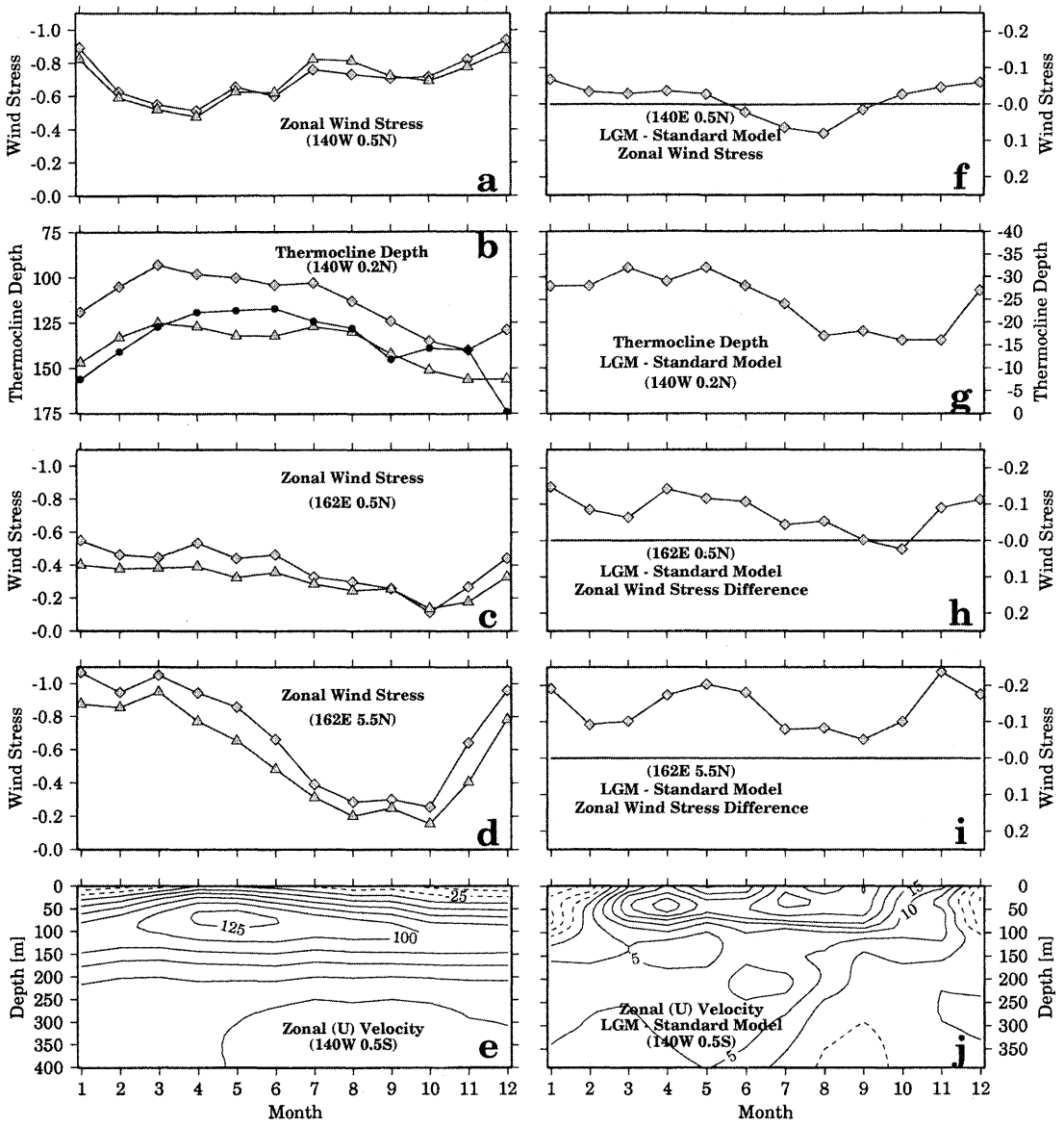

Figure 6. (a-e) Monthly plots are of standard and LGM model run thermocline depth, wind stress and zonal velocity (cm s^{-1}) (SMR values are in triangles and LGM values are diamonds). (f-j) Anomalies (LGM-SMR) for these parameters. For Figure 6b, thermocline depth (meters) at 140°W including values derived from the Levitus climatology [1982] (solid circles) are also included. Units are in dyne cm^{-2} for wind stress, meters below sea surface for thermocline depth, and cm s^{-1} for zonal velocity.

which seasonal variations in wind-driven thermocline depth in the west initiate the eastward propagation of Kelvin waves which modulate the thermocline depth in the CEP [*Philander and Pacanowski*, 1980, 1981; *McPhaden and Hayes*, 1990; *Murray et al.*, 1994]. Thus, paleoceanographic records should be interpreted in consideration of the notion that both local and remote wind forcing can explain changes in thermocline depth and other associated conditions such as biological productivity in the CEP [*Murray et al.*, 1994].

In response to increased zonal wind stress, both thermocline shoaling along the equator and off-equatorial thermocline subsidence are expected due to off-equatorial mass accumulation via Ekman drift [*Cane and Sarachik*, 1981]. At 6.5°N, in a zone between 130°W and the dateline, this general relationship holds true both in the SMR and the LGMR where thermocline subsidence increased (Figure 8). West of the dateline however, the off-equatorial response to stronger trade winds along the equator is quite different. Here our results support previous analytical and model results, which indicate the ocean's momentum balance is dominated by linear (vertical mixing), rather than non-linear (horizontal advection) processes [*Wacongne*,

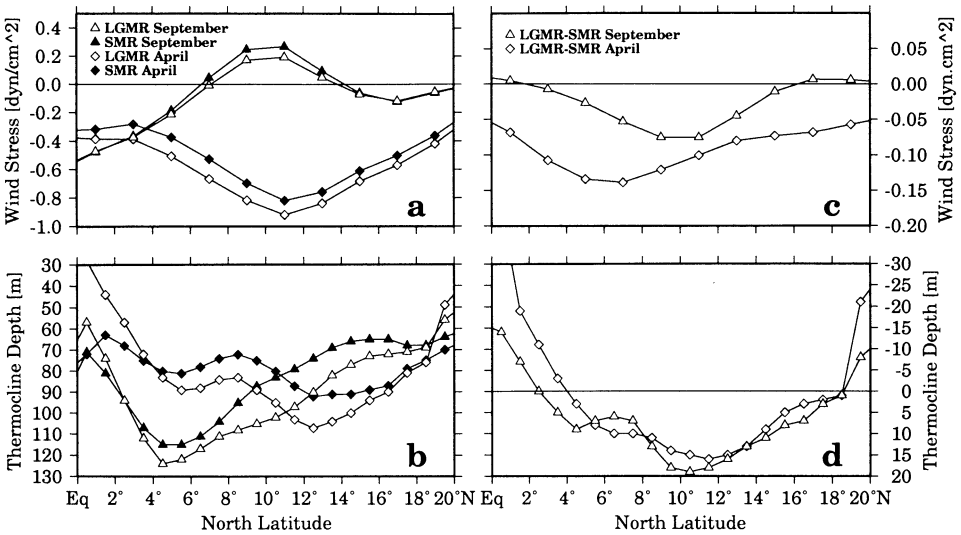

Figure 7. Model results of (a) zonal wind stress and (b) thermocline depth (April, diamonds; September, triangles) along a meridional transect at 120°W from the equator to 20°N. Anomalies for (c) wind stress and (d) thermocline depth of the model LGM minus the control (SMR).

1989, 1990; *Philander and Chao*, 1991]. In the face of stronger LGM simulated zonal winds the off-equatorial thermocline in general shoals relative to the SMR, seasonality is shifted in phase, and is offset by an increase in downward vertical mixing along the equator (Figure 8; see also Figures 9 and 10). SMR results indicate a phase lead of thermocline subsidence by ~2 months prior to the maxima in zonal winds (Figures 8a and 8b). This phase lead differs from analytic calculations which predict the thermocline response west of 180°W lead equatorial wind stress by roughly 5 months [*Cane and Sarachik*, 1981]. Furthermore, this phase lead disappears for the LGMR such that off-equatorial thermocline subsidence is in phase with equatorial winds.

4.2.2. Equatorial undercurrent. The annual average undercurrent velocity is stronger in the LGMR than in the SMR throughout the interior of the central Pacific (Figures 6e and 6j). Enhanced eastward velocity of the EUC retards the westward surface flow and concentrates it in the upper 100 m between 170°W and 120°W within the shallower thermocline. East of 110°W the progress of the EUC in the upper 75 m is slow in the LGMR relative to the SMR and consequently surface advection within the South Equatorial Current (SEC) is strengthened and advection of the Peru current into the equatorial region is enhanced in the LGMR. In the lower portion of the EUC, between 120 and 200 m depth, transport is moderately intensified in the EEP (Figure 5).

Seasonal variability in the EUC anomaly (at 140°W) (Figure 6j) appears to be a result of both local and remote wind forcing. Higher velocity of EUC through most of the year in the LGMR is related to generally stronger remote winds in the west Pacific (Figures 6h and 6i) which set up a stronger pressure gradient and eastward subsurface flow. However, the superimposed influence of seasonal variations in local wind help to explain the seasonality of the EUC anomaly (Figure 6f). In the boreal winter (December, January, and February), enhanced local wind forcing inhibits EUC eastward flow. Slower EUC flow at this time is not due to wind forcing in the western Pacific which is stronger throughout the year. In boreal summer (July, August, and September) anomalously strong eastward momentum of the EUC is related to weaker local wind forcing (Figures 6f and 6j). However, the strong anomaly in March and April is not associated with a similar weakening of local winds at that time and must be attributed to a stronger pressure gradient due to enhanced remote (western Pacific) winds (Figures 6h and 6i). In sum, the LGMR demonstrates that, as with the thermocline depth in the CEP, the EUC responds to changes in both remote and local wind forcing. This aspect of the dynamical response of the CEP to basin-wide changes in wind forcing is taken into account in the following sections in order to explain paleoceanographic observations.

5. Discussion

5.1. Regional Thermocline Depth Changes

The LGMR is designed to isolate the hydrographic response to the LGM wind stress anomaly; LGM boundary conditions have implicit but no direct influence on the outcome of the perturbed run since ocean-atmosphere feedbacks are not modeled. Comparison of data-based (transfer function) estimates of LGM thermocline depth [*Andreasen and Ravelo*, 1997] to those in the perturbed run are used here to evaluate if the regional response to the LGM wind anomaly is of pri-

mary importance to LGM tropical ocean dynamics (Figure 11). Despite discrepancies at a few sites, modeled and observed thermocline depth anomalies are in excellent agreement (of the same sign and of similar magnitude). Both the model and the transfer functions predict an increased equatorial thermocline tilt in the LGM relative to today, about 15 to 20 m shallower in the east (between 120° and 140°W) and about 15 to 20 m deeper in the west (between 160° and 180°E), little or no change east of 110°W along the equator, and a deeper thermocline north of the equator. Although, as described earlier, the model had a drift in the thermocline depth in the region south of 8°S, between 115°W and 125°W, both model and transfer functions predict that the LGM thermocline was approximately 30 m shallower in this region, with anomalies increasing toward the east. Overall, the model-data agreement is remarkable (Figures 11 and 9). Interestingly, calculations of thermocline depth response to LGM boundary conditions using a coupled model [*Bush and Philander*, 1998] both overestimate the magnitude and distort the zonal distribution of thermocline shoaling in the east and the deepening in the west (Figure 9). LGM distribution of the 18°C isotherm of the coupled model simulation suggest Walker circulation was too strong [*Bush and Philander*, 1998], though it remains unclear as to why this is so. This comparison indicates that the observed thermocline depth changes are best explained as a response to tropical wind forcing resulting from glacial boundary conditions which (slightly) modify existing tropical ocean-atmosphere interactions. In addition, the subtle changes which emerge in our LGMR result are from interactions between currents which are well-resolved in our model but poorly resolved in the coupled model. Below we present a more detailed analysis of what is driving hydrographic changes in the LGMR in the context of explaining sedimentary records of tropical paleoceanographic conditions.

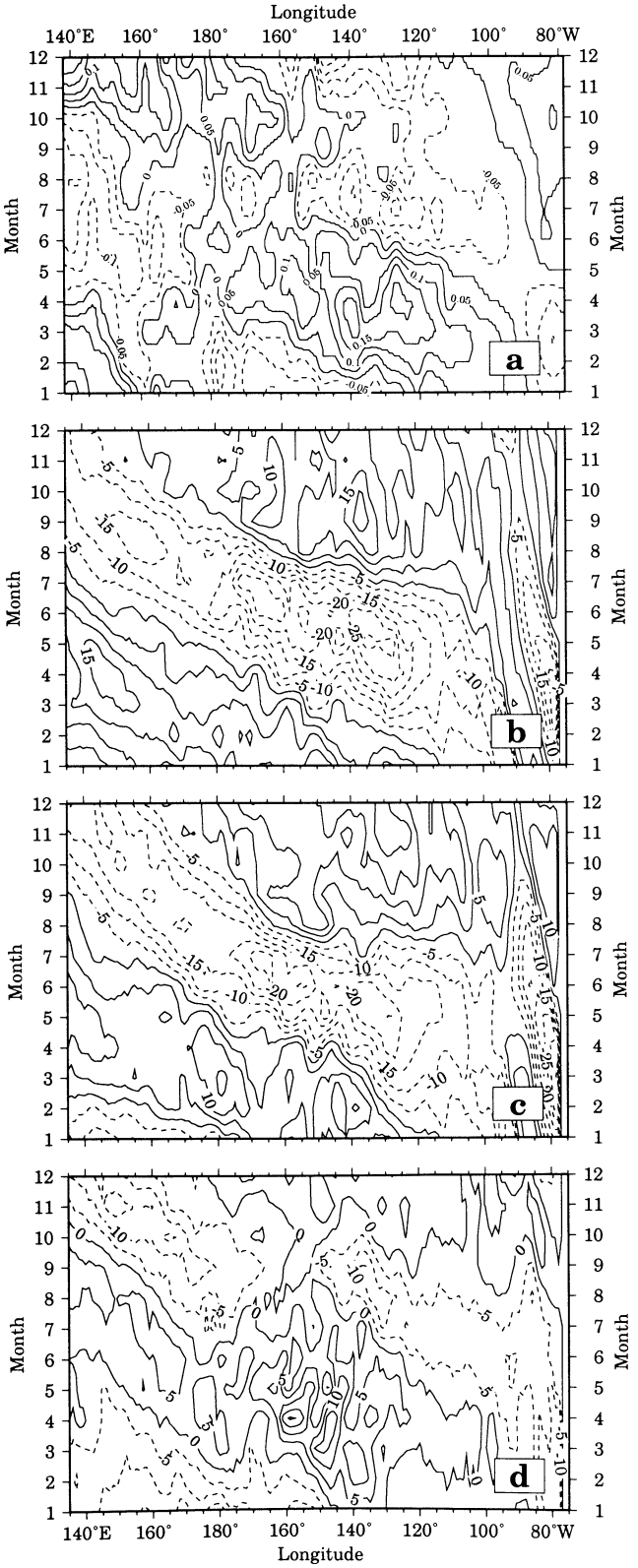

Figure 8. Off-equatorial thermocline depth response to equatorial winds. Equatorial Ekman drift driven by southeast trades should be associated with accumulation of off-equatorial mass and a thermocline subsidence. (a) Monthly departure of the zonal wind stress along the equator from the annual mean [*Hellerman and Rosenstein*, 1983]. (b) Monthly SMR departure of off-equatorial thermocline depth at 6.5°N from the SMR annual mean value. (c) Monthly LGMR departure of off-equatorial thermocline depth at 6.5°N from the LGMR annual mean. Positive values indicate a deeper thermocline than the mean. (d) Anomaly (LGMR-SMR) of the mean departures of thermocline depth from their respective annual means. Positive values indicate a relatively deeper LGMR thermocline than the SMR thermocline at a particular month and position.

5.2. North of the Equator

North of the equator, generally within the confines of the NECC and southern portion of the NEC, the LGMR predicts a deepening of the thermocline (Figures 4 and 7). While other studies have inferred a southward shift in the ITCZ [*Romine*, 1982; *Rea et al.*, 1986], the stronger NE trades centered at about 10°N (Figures 7a and 7c) in the A-MLO-LGM simulation are a result of more intense momentum transfer from

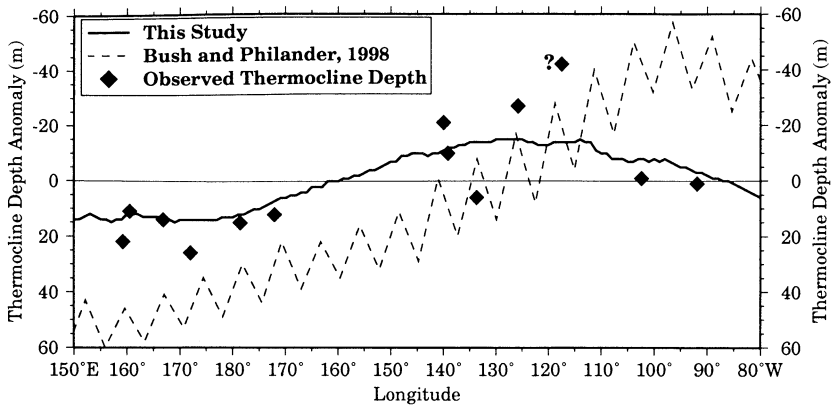

Figure 9. Ocean model LGM annual average annual thermocline depth anomaly along the equator for this study and for the LGM coupled model simulation of *Bush and Philander* [1998]. Diamonds are foraminiferal transfer function estimated thermocline depth [*Andreasen and Ravelo*, 1997] using sediment samples of LGM age from within 6° latitude of the equator. A negative thermocline depth anomaly indicate the LGM thermocline was shallower than either the model control run or Holocene thermocline depth estimate. An anomalous thermocline depth estimate next to the question mark is discussed in the text.

the western Atlantic across Central America into the Pacific (Figure 3c) and would be expected to result in a weakening of the NECC [*Wyrtki and Kilonsky*, 1984]. As expected, in the LGMR during the season (September) of maximum NECC flow, the velocity of the NECC (at its core at about 8°N) is reduced, divergence at its northern boundary is diminished, and the thermocline is deeper (centered at 10°N) (Figure 7d). The core of the NECC and the convergent downwelling at its southern boundary are actually shifted south (between about 8°-4°N) resulting in a deepening of the thermocline at these latitudes as well. In the opposite part of the year (April) the strongest winds in the LGMR are centered at 11°N as they are today (Figure 7a), but the largest anomaly is at 6°N. Thus deepening of the thermocline both north and south of the maximum NE trades and the core of the NEC results from the decrease in wind stress curl to the south and the increase in wind stress curl to the north.

Available data on past thermocline depth changes from this region are from sites located on the southern edge of the deep LGMR thermocline depth anomaly (Figure 4c). Isotopic analysis of multiple species of planktonic foraminifera at Ocean Drilling Program site 851 (2.46°N, 110.34°W) [*Ravelo and Shackleton*, 1995] indicates that the thermocline deepened in the LGM, consistent with the LGMR results. However, transfer functions estimate the thermocline depth shoaled by 42 m (at 3.2°N, 117.5°) 700 km to the west of ODP site 851

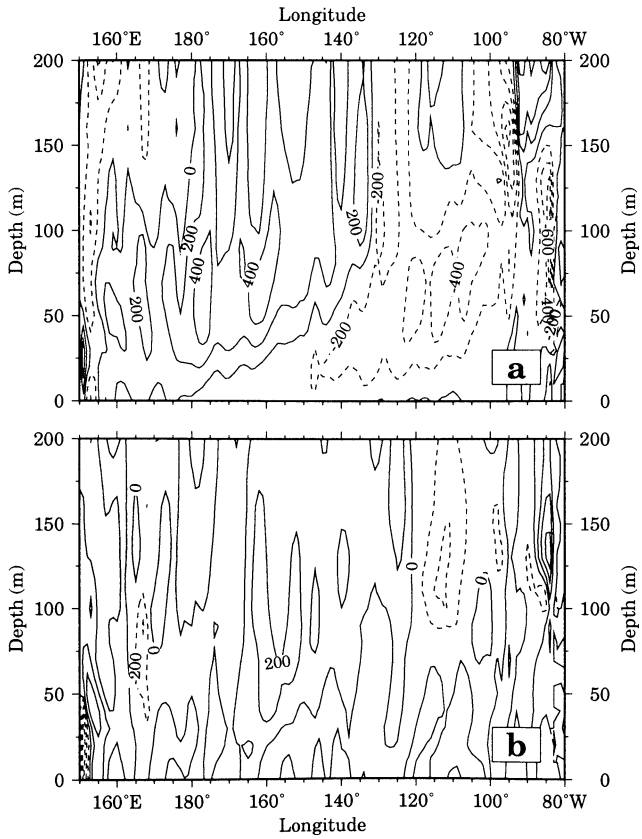

Figure 10. (a) Vertical velocity contours (at 200 cm d^{-1} intervals) along the equator for the SMR. Note that the downwelling between 95°W and 130°W is part of a strong meridional cell which upwells south and downwells at and to the north of the equator due to a strong cross-equatorial meridional wind stress component here (Figure 3) [*Philander and Delecluse*, 1983]. Strong equatorial upwelling is displaced south of the equator at ~3°S in this region. (b) Vertical velocity anomaly contour plot (LGMR-SMR, 200 cm d^{-1} contour interval). Positive contours indicate stronger upwelling. Increased LGMR entrainment from the deeper portions of the equatorial undercurrent are evident in the central equatorial Pacific between 150 and 160°W.

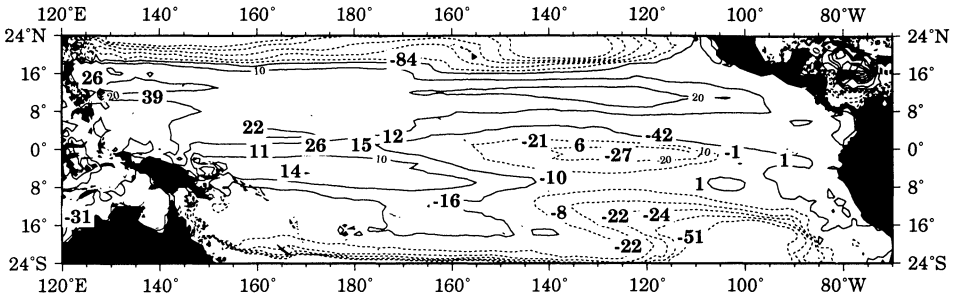

Figure 11. Thermocline depth anomaly for LGM-modern (discrete numbers) predicted by the foraminiferal transfer function. Positive (negative) values indicate thermocline depth deepened (shoaled) during the LGM. Background contours overlain are 4-year averaged model predicted thermocline depth anomalies (as in Figure 4).

[*Andreasen and Ravelo*, 1997] (Figure 11). This mismatch could be due to tropical instability waves arising from barotropic instability caused by shear between the NECC and SEC [*Cox*, 1980; *Hansen and Paul*, 1984], and resulting in episodes of high surface nutrient content and productivity [*Murray et al.*, 1994] that could support anomalous foraminifera production. In fact, in a set of cross-equatorial plankton tows (at 140°W), *Watkins et al.* [1996] found a unique assemblage containing relatively high abundances of *Neogloboquadrina dutertrei* in the surface water associated with a convergent front north of the equator. Other possible alternatives include partial dissolution which would result in higher abundances of this resistant species in the sediment sample. Transfer functions generally predict shallower thermocline depths when assemblages contain relatively high abundances of *Neogloboquadrina dutertrei*, whereas isotope-based estimates are not directly dependent on relative abundances of species. Or, because this region has high interannual variability, faunal assemblages could reflect a higher frequency of cold events [*Clement et al.*, 1999]. Overall, this one transfer function estimate (predicting 42 m shoaling of the thermocline) is the only data point that significantly contradicts, while nearby data support, the LGMR results. Thus we believe that the deep thermocline depth anomaly north of the equator represents LGM conditions accurately.

In the far east and north of the equator, the LGMR predicts a reduction in the intensity of upwelling (deepening of the thermocline) within the Costa Rica Dome (Panama Basin region) due to a dynamic response of the circulation to the wind stress anomaly. Deepening of the thermocline is supported by LGM observations of increased faunal SST [*Pisias and Mix*, 1997], a reduction in carbon accumulation [*Sarnthein et al.*, 1988] and a reduction in denitrification (depleted LGM δ^{15}N) [*Ganeshram and Pedersen*, 1998] in this region.

5.3. Southeast Tropical Pacific (Between 100°-130°W and 10°-25°S)

Hydrographic data and modeling studies demonstrate that there are modes of meridional transport between the subtropics and tropics along characteristic pathways. There is a low latitude-western boundary current (LLWBC) pathway with a transit time of >5 years and transport of roughly 14 Sv, and a more rapid (<5 years) "interior pathway" linking the eastern subtropics to the CEP thermocline with transports of roughly

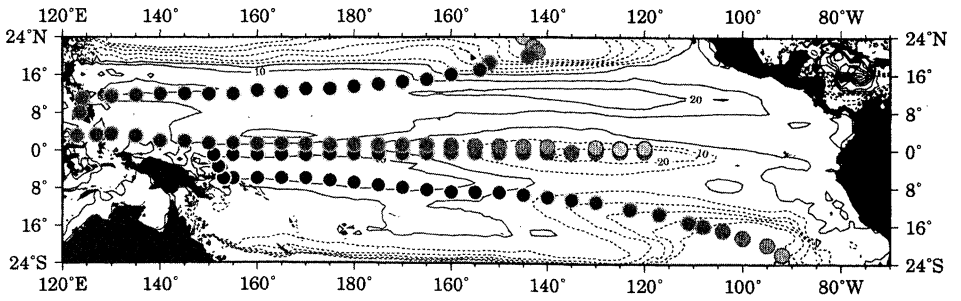

Figure 12. Model thermocline (18° isotherm) depth anomaly (LGM - standard model run) contour plot with shaded circles outlining the "low-latitude western boundary current" pathway linking the subtropics to the tropical thermocline [after *Gu and Philander*, 1997]. Shaded circles qualitatively reflect depth in the water column with darkest/(lightest) shades reflecting about 180/(25) m depth. Thermocline depth shoaling patterns in the northest and southeast tropical Pacific are matched by patterns seen in both the model and foraminiferal transfer function estimations.

12-16 Sv [*Johnson and McPhaden*, 1998; *Huang and Liu*, 1999]. As stated previously, the southeast tropical region is the only place where there is a drift in the LGMR over model run years 5-8, with the 18° isotherm shoaling by over 100 m. A LGMR thermocline depth anomaly pattern (Figure 12) occurs along the "LLWBC pathway" from the southeastern region (100°W and 25°S) where water parcels are subducted, advected to the northwest along isopycnal surfaces, and into the equatorial thermocline [*Gu and Philander*, 1997]. Subduction and transport of cooler subtropical waters may be responsible for the gradual shoaling of the 18° isotherm along the transport pathway. Shoaling of the 18° isotherm in the southeast during the LGM is actually predicted by foraminiferal transfer functions (Figure 11) and implies that subducted waters transported along the subtropical-tropical "LLWBC pathway" were indeed cooler in the LGM. A recent LGM simulation using a coupled ocean-atmosphere model [*Bush and Philander*, 1998] suggests that subtropical-to-tropical exchange accounts for ≈1-2°C tropical cooling. The transfer function estimate of significant thermocline depth shoaling west of Hawaii (Figure 11) and cooler SST in the North Pacific subtropical gyre [*Lee and Slowey*, 1999] may also indicate that meridional subsurface advection in the Northern Hemisphere was a contributor to tropical cooling.

While it seems that advection of cool water into the tropical thermocline may induce subsequent feedbacks on tropical climate, our results indicate that they are not a critical factor in determining thermocline depth. Except for in the southeast region as described above, our LGMR is not strongly influenced by the longer term effects of changes in the temperature of thermocline source water and does not include any subsequent feedbacks on the winds. However, because the model in still adjusting in the southeast region, the final equilibrium result is unknown. Nevertheless, there is excellent agreement between the pattern of observed and LGMR thermocline depth anomalies (Figure 11) indicating that much of the change in tropical thermocline structure and EUC strength in the LGM is due to intratropical wind forcing. This implies that extratropical oceanic exchange into the tropics may primarily alter thermocline and surface temperatures, while not resulting in significant changes in thermocline depths or EUC speed. This idea is consistent with process model experiments of *Liu and Philander* [1995].

5.4. Central Equatorial Pacific

In the equatorial Pacific, fluxes of organic carbon to the deep ocean are dependent on biological processes such as phytoplankton production, grazing, and export, and on physical processes that influence nutrient supply such as upwelling and advection [*Murray et al.*, 1994]. At the equator, upwelled water comes from a depth of 50 to 100 m. This source water reaches the equator along isopycnal surfaces from the north and south [*Wyrtki*, 1981] as part of vigorous meridional recirculation cells which occupy the upper water column within 5 degrees of the equator [*Philander et al.*, 1987]. Source water thermal and nutrient properties are influenced by the impingement and mixing of thermocline waters on these cells [*Murray et al.*, 1994] and by the advection of major and trace nutrients into the thermocline via the EUC [*Coale et al.*, 1996a]. For example, iron entrained within the EUC into the mixed layer of the CEP can produce large chain diatom blooms capable of increasing carbon export fluxes potentially influencing climate change [*Coale et al*, 1996b]. Thus biological production can be influenced not only by local wind forcing through its effects on subsurface mixing with nutrient sources but also by remote wind forcing through its effects on the thermocline depth and the strength and compositional character of the EUC.

We compiled organic carbon accumulation records and transformed them into estimates of new productivity in the LGM, relative to today, using the equation of *Sarnthein et al.* [1988] (Figure 13). We reproduce the well-known band of higher than modern productivity across the equatorial Pacific (Figure 13b). In the LGMR the thermocline is shallow relative to today in the CEP (between 160° and 110°W), and consequently, the EUC outcropped to the west of where it does today (Figure 13c) and entrainment of water from the relatively nutrient rich deep EUC increased by ~50% (Figure 10). Thus in the LGM the CEP surface water nutrient content could have been significantly enhanced by increased entrainment of nutrient-rich EUC water into the wind-mixed layer because of a shallower thermocline position without changing local winds. In sum the LGMR has a hydrographic response which is consistent with the observed enhanced LGM CEP productivity.

Wind anomalies in the western Pacific drive the hydrographic changes in the CEP during the LGM just as they drive the seasonal cycle of productivity in the CEP in the modern ocean [*Murray et al.*, 1994]. Therefore geologic records of productivity changes in the CEP are not necessarily expected to be coherent with local wind forcing. In the CEP (at 140°W), *Pisias and Rea* [1988] show that their radiolarian-based "equatorial divergence index" is coherent with changes in eolian grain size (wind strength) at a period of 31 kyr, a combination tone of Milankovitch variability. However, neither the percentage of "divergence" species [*Pisias and Rea*, 1988] nor CEP SST [*Lyle et al.*, 1992] is related to local wind strength at Milankovitch periods (100 kyr for radiolaria and 23 kyr cycles for both). Because the CEP is sensitive to remote forcing and its influence on thermocline depth and the EUC, it is not surprising that biological and physical changes in the CEP could be decoupled from changes in local wind strength as documented by these studies.

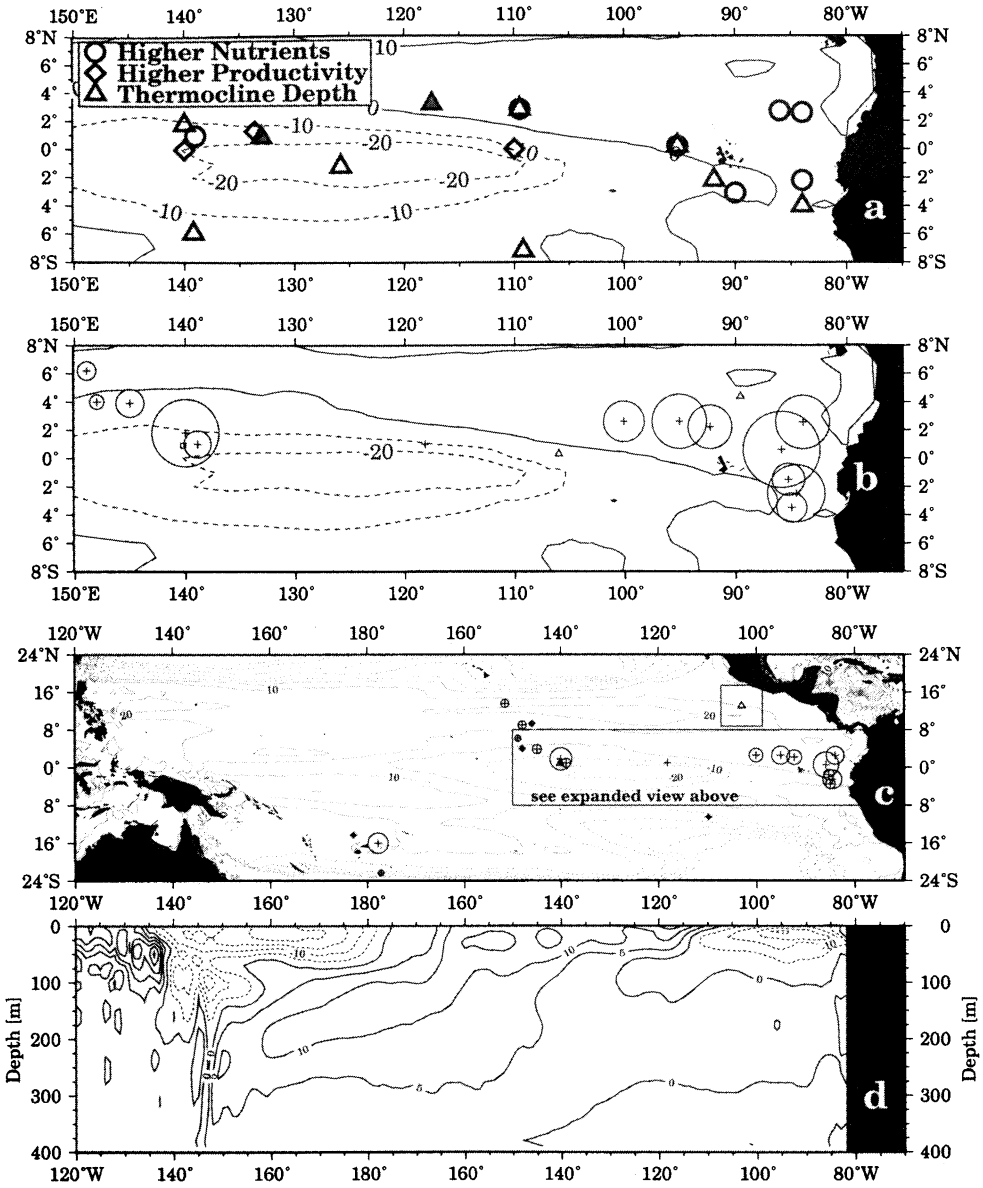

Figure 13. (a) Summary of eastern equatorial Pacific paleoceanographic hydrographic, productivity, and nutrient studies. Contour lines are the model-predicted thermocline depth anomalies. Note the area displayed focuses on a limited equatorial geographic regions outlined by the box in Figure 13c. Symbols group a variety of proxy data. Proxies of thermocline depth (triangles) are open when they agree with the model estimates and shaded when they do not agree (data from *Andreasen and Ravelo* [1997], *Ravelo and Shackleton*, [1995], *Farrell et al.*, [1995]b, and *Patrick and Thunell*, [1997]). Higher nutrients proxies are from estimates of pCO_2 of bulk organic matter [*Jasper et al.*, 1994], boron isotopes of planktonic foraminifera [*Sanyal et al.*, 1997], and nitrogen isotopic studies of bulk sediments [*Farrell et al.*, 1995b]. (b and c) Summary of LGM minus Holocene new productivity estimates, based upon organic carbon burial as formulated by *Sarnthein et al.* [1988]. Circles (centered on pluses) reflect greater LGM new production than the Holocene, whereas squares (centered upon a triangle) reflect lower new production. The size of the symbol (circle or square) indicates the magnitude of difference between the LGM and Holocene. In the background is the LGMR-SMR surface anomaly contour plot of thermocline depth. (b) is a subset of Figrure 13c and focuses on the same eastern equatorial Pacific region as Figure 13a. Data are from *Sarnthein et al.*, [1988, and references therein], *Rea et al.*, [1990, 1991], and *Emeis et al.* [1995]. (d) Anomaly contour map of LGMR minus standard model run zonal (u component) velocity (contours in cm s^{-1}).

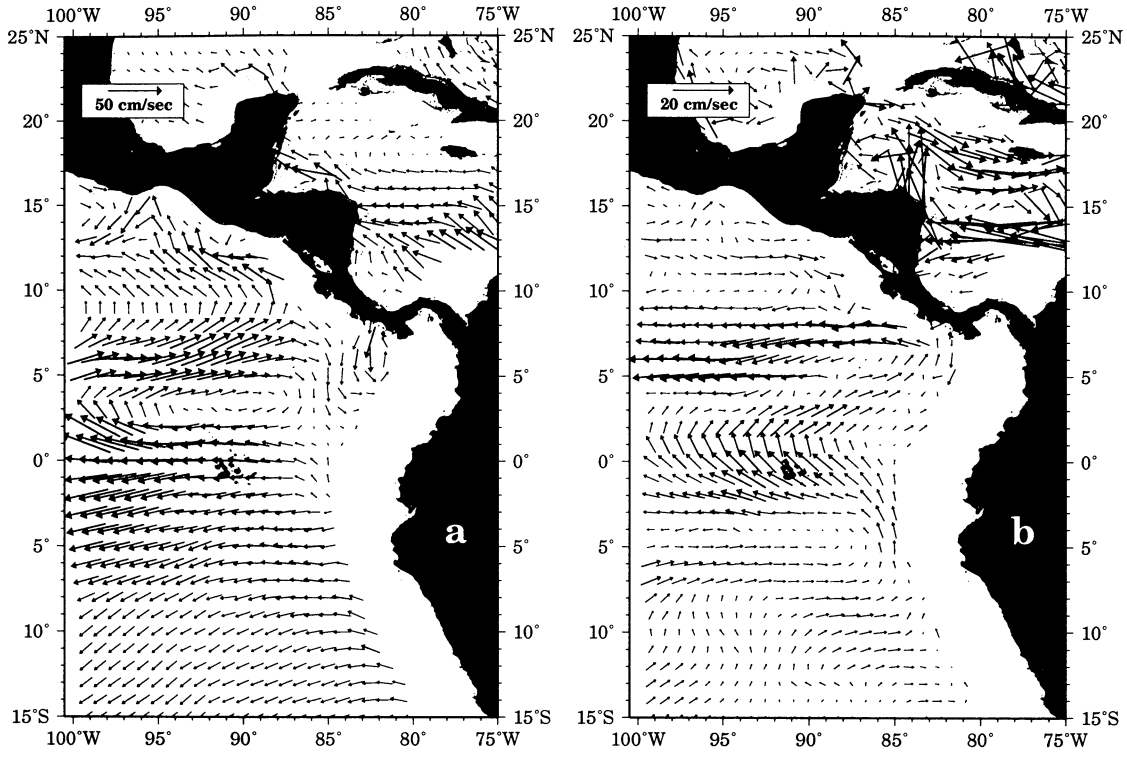

Figure 14. (a) Model surface current velocity (cm s^{-1}) vector plots for the SMR. (b) Surface current anomaly vector plot (LGMR-SMR) in the far eastern equatorial Pacific. Note the increased advection of Peru upwelled water in the the equatorial region at the expense of direct westward Ekman transport off Peru. Also note the increase in cross equatorial advection into the northern hemisphere.

5.5. Eastern Equatorial Pacific (East of 100°W)

In the LGMR the large eastward flow anomaly in the CEP and large westward flow anomaly in the far-EEP in the upper 100 m is a consequence of a westward shift in the shoaling of the core of the EUC (Figure 5). Drag of the EUC by overlying easterly surface currents in the CEP curtailed the EUC's influence in the far-EEP. Reduced EUC strength is compensated by stronger equatorward advection by the cold, turbid Peru Current into the equatorial zone to 105°W and westward along the equator (Figure 14).

In addition, cross-equatorial flow is greater in the LGMR because of a weakening of the salinity front located just north of the equator today. In the modern ocean, Peruvian coastal upwelled water is advected west as evidenced by a nutrient maximum ("tongue") south of the equator at 7°S [*Philander et al.*, 1987; *Toggweiler and Carson*, 1995]. This nutrient tongue is constrained to the north by a front between cool saline Equatorial Surface Water originating from the Peru Current and EUC, and warm, fresher Tropical Surface Water north of the equator [*Wyrtki*, 1966] originating from the NECC, continental runoff, and excess precipitation over evaporation in the Costa Rica Dome region [*Dietrich*, 1957]. This salinity gradient limits cross-equatorial mass exchange despite strong cross-equatorial winds in this region today. Since the LGMR does not incorporate hydrological (E-P) changes, it cannot be used to accurately predict the influence of hydrologic changes on the LGM surface salinity field. However, a reduction of the NECC results in higher than modern salinity north of the equator, a more ephemeral equatorial front, and greater cross-equatorial advection of high nutrient water derived from the Peru Current.

Data-based paleoceanographic studies of LGM conditions in the far EEP indicate that SSTs were cooler than today [*CLIMAP*, 1981; *Pisias and Mix*, 1997; *Patrick and Thunell*, 1997; *Mix et al.*, 1999] while the thermocline depth was relatively unchanged [*Andreasen and Ravelo*, 1997; *Patrick and Thunell*, 1997; *Faul et al.*, 2000]. Our model results substantiate the notion that hydrographic changes in the far-EEP were constrained to the sea surface and were related to advection of cool waters rather than from shoaling of the EUC or thermocline in the far-EEP.

How does the proposed and modeled hydrographic changes (Figure 14) explain enhanced paleoproductivity throughout the EEP in the LGM (Figure 13)? While the cause remains unclear, changes in the delivery of nutrients to the far-EEP must be considered. In the

modern ocean, the EUC encroaches upon and bifurcates about the Galápagos Islands [*Lukas*, 1986] and part of the southern branch is entrained into the southward Peru-Chile Undercurrent [*Wyrtki*, 1963] becoming an important component of source waters upwelled off of Peru [*Wyrtki*, 1963; *Brockmann et al.*, 1980; *Toggweiler et al.*, 1991]. Because nutrient rich water within the deep EUC are thought to originate from Subantarctic Mode Water (SAMW), changes in the nutrient composition of Mode Water have been proposed as an explanation for increased productivity in the far-EEP at the LGM [*Toggweiler et al.*, 1991; *Toggweiler and Carson*, 1995]. Indeed surface ocean carbon isotopic records might link the Subantarctic Pacific and EEP presumably via SAMW, though preformed $\delta^{13}C$ air-sea overprints complicate establishing a nutrient link between the two regions [*Shackleton et al.*, 1983; *Ninnemann and Charles*, 1997]. Our results, in combination with data-based evidence for no change in the thermocline depth in the EEP, are consistent with this idea. Alternatively, there may have been stronger near-coastal upwelling (where we have no thermocline depth reconstructions) and advection of nutrient-rich waters into the EEP. Most importantly, the breakdown in the cross-equatorial salinity gradient could explain the cross-equatorial advection of nutrient rich waters resulting in enhanced paleoproductivity throughout the EEP rather than only within the modern cool nutrient tongue (Figure 13).

The idea that enhanced biological productivity in the LGM was stimulated by iron seeding from increased aluminosillicate deposition [*Boyle*, 1983; *Molina-Cruz*, 1977] due to drier conditions along the west coast of the South American continent [*Heusser and Shackleton*, 1994] is not supported by a number of other studies. For example, the LGM was a period of lower nutrient utilization in the EEP [*Farrell et al.*,1995b; *Sanyal et al.*, 1997] and CEP [*Jasper et al.*, 1994], rather than higher nutrient utilization as would be expected from iron fertilization during the LGM. Higher LGM major nutrient concentrations in surface waters [*Farrell et al.*, 1995a, 1995b; *Ravelo and Shackleton*, 1995; *Faul et al.*, 2000] resulted in higher net carbon export [*Sarnthein et al.*, 1988; *Pedersen*, 1983; *Lyle et al.*, 1988], while efficiency of nutrient utilization actually decreased [*Farrell et al.*, 1995b]. Furthermore, even subnanomolar additions of trace nutrient iron concentrations in equatorial Pacific waters lead to substantial phytoplankton response, particularly in diatoms [*Coale et al.*, 1996b]. Yet in the LGM, as in the modern ocean, biological productivity in the EEP was a tightly coupled production-grazing-regeneration community dominated by small nanoplankton and picoplankton [*Murray et al.*, 1994; *Lyle et al.*, 1988; *Farrell et al.*, 1995b].

Overall, observed paleoceanographic conditions in the LGM are consistent with modeled hydrographic changes in which the EUC was weaker in the EEP and easterly and cross-equatorial flow was enhanced. The EEP had enhanced nutrient concentrations resulting from a stronger supply of nutrients from the Peru Current, either because of an increase in nutrient concentrations in upwelled waters or because of stronger advection throughout the EEP. Neither regional upwelling in the EEP nor the supply of trace nutrients relative to major nutrients were enhanced in the LGM. Thus, the LGM conditions in the EEP were different than the CEP where the thermocline was shallower and higher paleoproductivity could be explained by greater upwelling of nutrient-enriched EUC water.

5.6. Mechanisms of tropical SST and paleoproductivity change

Paleoceanographic time series of near-equatorial SST and organic carbon burial (paleoproductivity) [*Pedersen*, 1983; *Lyle et al.*, 1992] indicate that changes in SST and paleoproductivity were out of phase [Lyle, 1988; *Lyle et al.*, 1992; *Rea et al.*, 1991; *Emeis et al.*, 1995]. Minima in SST lead maxima in organic carbon burial at all orbital periods (23, 41, 100 kyr) (Figure 15). Since nutrients do not limit phytoplankton production in the equatorial Pacific Ocean [e.g., *Chavez et al.*, 1990], *Lyle et al.* [1992] argued that maxima in biogenic particle flux might reflect increases in nutrient utilization unrelated to upwelling/advection while minima in SSTs might reflect upwelling or advection of cool waters. However, as discussed above, higher surface nutrient concentrations and therefore higher paleoproductivity in the LGM resulted from hydrographic changes: a shallower position of the EUC in the CEP and greater lateral advection of nutrient rich waters in the EEP. Thus we suggest that tropical SST minima are primarily forced by early radiative changes in the tropics [*Imbrie et al.*, 1992; *Broecker and Henderson*, 1998] rather than by circulation changes. Alternatively, tropical SST minima may be related to cooling of the thermocline [e.g., *Gu and Philander*, 1997; *Bush and Philander*, 1998] without a concomitant change in nutrient flux into the CEP and EEP. The lag of organic carbon burial maxima relative to SST minima reflect the tropical Pacific wind-driven hydrographic adjustment to peak glacial conditions such as ice sheet size and North Atlantic SST (which also lag tropical SST minima [*Imbrie et al.*, 1992]).

One further implication of the fact that SST changes are out of phase with hydrographic/productivity changes is that mechanisms that alter SST are decoupled from the dynamical forcing of the cross-basinal tilt of the thermocline. Generating long records of thermocline depth, paleoproductivity, and SST at locations across the Pacific would confirm this fundamental idea. Given the strong coupling between cross-basinal SST gradients, Walker circulation, and cross-basinal tilt in the thermocline that exists in the modern ocean, how might we explain that SSTs in the EEP were decoupled from thermocline depth changes? The most obvious possi-

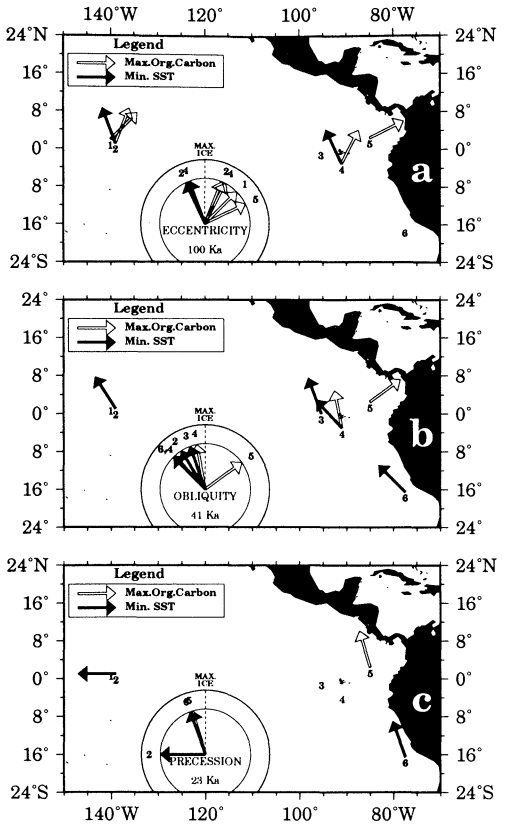

Figure 15. Phase wheel diagrams and position maps of sea surface temperature and organic carbon accumulation time series studies illustrating Milankovitch cycles in the tropical Pacific for (a) eccentricity, (b) obliquity, and (c) precession. The phase wheel diagrams illustrate relative cyclic leads/lags at Milankovitch periodicities. Vectors rotated clockwise of maximum ice volume (vertical dashed line) lag ice volume. Note that minima in SST typically lead maximum ice volume and maxima in organic carbon accumulation (paleoproductivity). Data are from 1, *Rea et al.* [1991], 2, *Lyle et al.* [1992], 3,6, *Pisias and Mix*, [1997], 4, *Emeis et al.*, [1995], 5, *Lyle*, [1988].

bility is that alterations in Walker circulation did not occur, otherwise tight coupling/synchronism between changes in SST and cross-basinal thermocline tilt would be expected. *Liu and Huang* [1997] determined that the zonal SST gradient is presently at or near saturation (i.e., intensifying winds or currents cannot further increase the gradient). Kinematics (i.e., stronger equatorial currents) act to cool the warm pool and thus the tropics as a whole which thereby act to regulate coupling strength by reducing differential latitudinal heating. Thus, an initial change, whether it be radiatively forced or due to cooler waters being subducted into the thermocline outside the tropics, might result in cooling of the entire tropics, but not of the cross-basinal SST nor thermocline gradients. Afterward, the tropical wind field response to high-latitude glacial conditions could have forced the dynamical response of the thermocline and altered paleoproductivity without significant additional changes in SST.

Maintenance of the coupling strength of Walker circulation, as suggested above, requires that the east-west temperature gradient in the LGM was similar to today. Is there evidence for this? Open ocean paleoceanographic SST proxies give different answers to this question. Some oxygen isotopic data from surface dwelling planktonic foraminifera LGM indicate that cross-basinal SST gradients were generally very similar to today with perhaps a slight cooling in the east [*Broecker*, 1986; *Farrell et al.*, 1995a], while others suggest the gradient was slightly reduced [*Patrick and Thunell*, 1997]. Faunal-based estimates indicate a stronger cross-basinal SST gradient [*Moore et al.*, 1980; *CLIMAP*, 1976, 1981; *Thunell et al.*, 1994; *Pisias and Mix*, 1997; *Mix et al.*, 1999]; however, fauna may not be sensitive enough to SST to make precise SST estimates in the warm pool [*Prell*, 1985; *Le and Shackleton*, 1994; *Andreasen and Ravelo*, 1997]. Finally, Mg/Ca analyses of planktonic foraminifera predict only a slightly greater (0.5°C) cross-basinal temperature gradient during the LGM while none is implied by $U_{37}^{K'}$ alkenone paleothermometry [*Lea et al.*, 1998; *Emeis et al.*, 1995a, *Lyle et al.*, 1992, *Rosell-Melé et al.*, 1998].

Overall, given the problems with faunal-based estimates particularly in the western warm pool, the existing data mostly indicates that in the LGM, the cross-basinal SST gradient was very close to modern. Certainly, future studies that indicate uniform cooling across the tropical Pacific would help to support the idea that the enhanced paleoproductivity and cross-basinal thermocline tilt was a response to remotely forced winds in the LGM, rather than to enhanced Walker Circulation.

6. Conclusions

1. High-resolution ocean model estimated thermocline depth display general agreement both in space and amplitude with thermocline depth estimates by foraminiferal transfer function for the LGM. This includes replicating the increased east-west thermocline slope along the equator reminiscent of an La Niña style circulation during the LGM. However, wind anomalies are remote, and unlike La Niña, the ocean model simulation replicates this pattern while maintaining winds similar to today over the southeastern, central, and eastern Pacific Ocean.

2. Our model results indicate the LGM EUC influence on productivity was redistributed in the tropical Pacific. In the CEP the EUC outcropped further west than today. In the EEP the EUC weakened which allowed for increased advection of the Peru Current in the far-EEP and a reduction of Peruvian upwelled water transported due west into the SEC. Comparison of our model results with existing paleoceanographic studies are favorable. Inferred higher LGM salinity north of

the equator in the far-EEP results from a weaker NECC and reduced continental runoff and allows for greater cross-equatorial flow of high-nutrient Peru Current waters in the far-EEP, potentially fueling increased LGM productivity observed in this region.

3. Adjustment of Walker circulation cannot explain the synthesis of paleoceanographic data, particularly the lag of paleoproductivity changes behind SST changes. In fact, lack of major changes in SST gradients imply Walker Circulation stasis. More SST data are needed to substantiate this idea.

4. Changes in atmospheric circulation simulated by an AGCM coupled to a slab ocean, occurring in response to LGM ice sheets, greenhouse gases, and orbital forcing, can explain much of the observed regional variability, even in the absence of explicit air-sea feedbacks.

Acknowledgments. We are grateful for insightful conversations and criticism of George Philander, Mitch Lyle, Adina Paytan, Matt Huber, and Mark Wells which improved this manuscript. Andy Bush graciously provided results of his coupled LGM simulation which we have included in our study. Reviews by Mitch Lyle and one anonymous referee were thoughtful and improved the manuscript. Greg Lambert at GFDL helped to execute the model experiments and kindly provided guidance and software which facilitated analysis of the model output. This research was supported by the Earth Sciences Board Regents Fellowship at University of California, Santa Cruz, and by a grant from the Geological Society of America (to D.H.A.) and by National Science Foundation grants ATM-9217034 and OCE-9811633 and a Petroleum Research Fund grant ACS-PRF-26743-GB8 (to A.C.R.).

References

Andreasen, D. J., and A. C. Ravelo, Tropical Pacific Ocean thermocline depth reconstructions for the last glacial maximum, *Paleoceanography*, *12*, 395–413, 1997.

Arrhenius, G., Sediment cores from the east Pacific, *Rep. Swed. Deep Sea Exped., 1947-1949*, *5*, 1–228, 1952.

Arrhenius, G., Rate of production, dissolution and accumulation of biogenic solids in the ocean, *Palaeogeog. Palaeoclimatol. Palaeoecol.*, *67*, 119–146, 1988.

Barber, R. T., and F. P. Chavez, Regulation of primary productivity rate in the equatorial Pacific, *Limnol. Oceanogr.*, *36*, 1803–1815, 1991.

Boyle, E. A., Chemical accumulation variations under the Peru current during the past 130,000 years, *J. Geophys. Res.*, *88*, 7667–7680, 1983.

Broccoli, A. J., Tropical cooling at the Last Glacial Maximum: An atmosphere-mixed layer ocean model simulation, *J. Clim.*, *13*, 951–976, 2000.

Brockman, C., E. Fahrbach, A. Huyer, and R. L. Smith, The poleward undercurrent along the Peru Coast: 5-15°S, *Deep Sea Res. Part I*, *27*, 847–856, 1980.

Broecker, W. S., Oxygen isotope constraints on surface ocean temperatures, *Quat. Res.*, *26*, 121–134, 1986.

Broecker, W. S., and G. M. Henderson, The sequence of events surrounding Termination II and their implications for the cause of glacial-interglacial CO_2 changes, *Paleoceanography*, *13*, 352–364, 1998.

Bush, A. B. G., and S. G. H. Philander, The role of ocean-atmosphere interactions in tropical cooling during the Last Glacial Maximum, *Science*, *279*, 1341–1344, 1998.

Cane, M. A., and E. S. Sarachik, The response of a linear baroclinic equatorial ocean to periodic forcing, *J. Mar. Res.*, *39*, 651–693, 1981.

Chavez, F. P., and R. T. Barber, An estimate of new production in the equatorial Pacific, *Deep Sea Res. Part I*, *34*, 1229–1243, 1987.

Chavez, F. P., K. R. Buck, and R. T. Barber, Phytoplankton taxa in relation to primary production in the equatorial Pacific, *Deep Sea Res. Part I*, *37*, 1733–1752, 1990.

Clement, A. C., R. Seager, and M. A. Cane, Orbital controls on the El Niño/Southern Oscillation and the tropical climate, *Paleoceanography*, *14*, 441–456, 1999.

Climate: Long-Range Investigation Mapping Prediction (CLIMAP) Project Members, The Surface of the ice-age Earth, *Science*, *191*, 1131–1137, 1976.

Climate: Long-Range Investigation Mapping Prediction (CLIMAP) Project Members, Seasonal reconstructions of the Earth's surface at the Last Glacial Maximum, *Map and Chart Ser.*, *MC-36*, pp. 1–18, Geol. Soc. of Am., Boulder, Colo., 1981.

Coale, K. H., S. E. Fitzwater, R. M. Gordon, K. S. Johnson, and R. T. Barber, Control of community growth and export production by upwelled iron in the eqatorial Pacific Ocean, *Nature*, *379*, 621–624, 1996a.

Coale, K. H. et al., A massive phytoplankton bloom induced by an ecosystem-scale iron fertilization experiment in the equatorial Pacific Ocean, *Nature*, *383*, 495–501, 1996b.

Cox, M. D., Generation and propogation of 30-day waves in a numerical model of the Pacific, *J. Phys. Oceanog.*, *10*, 1168–1186, 1980.

Dietrich, G., *Allgemeine Meereskunde*, Borntraeger, Berlin, Germany, 1957.

Dijkstra, H. A., and J. D. Neelin, Ocean-Atmosphere Interaction and the Tropical Climatology, II: Why the Pacific cold tounge is in the east, *J. Clim.*, *8*, 1343–1359, 1995.

Emeis, K.-C., H. Doose, A. C. Mix, and D. Schulz-Bull, Alkenone sea-surface temperatures and carbon burial at site 846 (eastern equatorial Pacific Ocean): The last 1.3 M.Y., *Proc. Ocean Drill. Program, Sci. Res.*, edited by N. G. Pisias et al., vol. 138, 605–613, 1995.

Farrell, J. W., D. W. Murray, V. S. McKenna, and A. C. Ravelo, Upper ocean temperature and nutrient contrasts inferred from Pleistocene planktonic foraminifer $\delta^{18}O$ and $\delta^{13}C$ in the eastern equatorial Pacific, *Proc. Ocean Drill. Program, Sci. Res.*, edited by N. G. Pisias et al., vol. 138, 289–311, 1995a.

Farrell, J. W., T. F. Pedersen, S. E. Calvert, and B. Nielsen, Glaical-interglacial changes in nutrient utilization in the equatorial Pacific Ocean, *Nature*, *377*, 514–517, 1995b.

Faul, K. L., A. C. Ravelo, and M. L. Delaney, Reconstruction of upwelling, productivity, and photic zone depth in the eastern equatorial Pacific Ocean using planktonic foraminiferal stable isotopic ratios and abundances, *J. Foraminiferal Res.*, *30*, 110–125, 2000.

Ganeshram, R. S., and T. F. Pedersen, Glacial-interglacial variability in upwelling and bioproductivity off NW Mexico: Implications for quaternary paleoclimate, *Paleoceanography*, *13*, 634–645, 1998.

Ganeshram, R. S., T. F. Pedersen, S. E. Calvert, and J. W. Murray, Large changes in oceanic nutrient inventories from glacial to interglacial periods, *Nature*, *376*, 1995.

Gu, D. F., and S. G. H. Philander, Interdecadal climate fluctuations that depend on exchanges between the tropics and extratropics, *Science*, *275*, 805–807, 1997.

Guilderson, T. P., R. G. Fairbanks, and J. Rubenstone, Tropical temperature variations since 20,000 years ago; modulating interhemispheric climate change, *Science*, *263*, 663–665, 1994.

Guilderson, T. P., and D. P. Schrag, Abrupt shift in subsur-

face semperatures in the tropical Pacific associated with changes in El Niño, *Science*, *281*, 240–243, 1998.

Halpern, D., A Pacific equatorial temperature section from 172°E to 110°W during winter and spring 1979, *Deep Sea Res. Part I*, *27*, 931–940, 1980.

Hansen, D. W., and C. A. Paul, Genesis and effects of long waves in the equatorial Pacific, *J. Geophys. Res.*, *89*, 10,431–10,440, 1984.

Harrison, D. E., On climatological monthly mean wind stress and wind stress curl fields over the world ocean, *J. Clim.*, *2*, 57–79, 1989.

Hellerman, S., and M. Rosenstein, Normal monthly windstress over the world oceans with error estimates, *J. Phys. Oceanog.*, *13*, 1093–1104, 1983.

Heusser, L. E., and N. J. Shackleton, Tropical climatic variation on the Pacific slopes of the Equadorian Andes based on a 25,000-year pollen record from deep-sea sediment core TRI-163-31B, *Quat. Res.*, *42*, 222–225, 1994.

Huang, B. Y., and Z. Y. Liu, Pacific subtropical-tropical thermocline water exchange in the National Centers for Environmental Prediction ocean model, *J. Geophys. Res.*, *104*, 11065–11076, 1999.

Imbrie, J., et al., On the structure and origin of major glaciation cycles, 1, Linear responses to Milankovitch forcing, *Paleoceanography*, *7*, 701–738, 1992.

Jasper, J. P., J. M. Hayes, A. C. Mix, and F. G. Prahl, Photosynthetic fractionation of $\delta^{13}C$ and concentrations of dissolved CO_2 in the central equatorial Pacific during the last 255,000 years, *Paleoceanography*, *9*, 781–798, 1994.

Johnson, G. C., and M. J. McPhaden, Interior pycnocline flow from the subtropical to the equatorial Pacific, *EOS Trans. AGU*, *79(45)*, Fall Meet. Suppl., F484, 1998.

Knauss, J. R., Further measurements and observations of the Cromwell Current, *J. Mar. Res.*, *24*, 205–240, 1966.

Le, J., and N. J. Shackleton, Reconstructing paleoenvironment by transfer function; model evaluation with simulated data, *Mar. Micropaleontol.*, *24*, 187–199, 1994.

Lea, D. W., D. K. Pak, A. Davé, and H. J. Spero, Using Mg-Paleothermometry to reconstruct glacial sea-surface temperatures, *EOS Trans. AGU*, *79(45)*, Fall Meet. Suppl., F471, 1998.

Lee, K., and N. C. Slowey, Cool surface waters of the subtropical North Pacific Ocean during the last glacial, *Nature*, *397*, 512–514, 1999.

Levitus, S., Climatological atlas of the world ocean, *NOAA Prof. Pap.*, *13*, 73 pp., 1982.

Levitus, S., and T. P. Boyer, *World Ocean Atlas 1994*, Nat. Oceanic and Atmos. Admin., Silver Spring, Md., 1994.

Liu, Z., and B. Y. Huang, A coupled theory of tropical climatology: Warm pool, cold tongue, and Walker circulation, *J. Clim.*, *10*, 1662–1679, 1997.

Liu, Z., S. Shin, P. Behling, W. Prell, M. Trend-Staid, S. P. Harrison, and J. Kutzbach, Dynamical and observational constraints on tropical Pacific sea surface temperatures at the Last Glacial Maximum, *Geophys. Res. Lett.*, *27*, 105–108, 2000.

Liu, Z. Y., and S. G. H. Philander, How different wind stress patterns affect the tropical subtropica circulations of the upper ocean, *J. Phys. Oceanog.*, *25*, 449–462, 1995.

Lukas, R., The termination of the equatorial undercurrent in the eastern Pacific, *Prog. Oceanogr.*, *16*, 63–90, 1986.

Lukas, R., and E. Firing, The Rossby wave in the central Pacific Ocean, *J. Phys. Oceanog.*, *15*, 55–67, 1985.

Lyle, M. W., Climatically forced organic carbon burial in equatorial Atlantic and Pacific Oceans, *Nature*, *335*, 529–532, 1988.

Lyle, M. W., D. W. Murray, B. P. Finney, J. Dymond, J. M. Robbins, and K. Brooksforce, The record of late Pleistocene biogenic sedimentation in the eastern tropical Pacific Ocean, *Paleoceanography*, *3*, 39–59, 1988.

Lyle, M. W., F. G. Prahl, and M. A. Sparrow, Upwelling and productivity changes inferred from a temperature record in the central equatorial Pacific, *Nature*, *355*, 812–815, 1992.

McPhaden, M. J., and S. P. Hayes, Variability in the eastern equatorial Pacific Ocean during 1986-1988, *J. Geophys. Res.*, *95*, 13,195–13,208, 1990.

McPhaden, M. J., and B. A. Taft, On the dynamics of seasonal and intraseasonal variability in the eastern equatorial Pacific, *J. Phys. Oceanog.*, *18*, 1713–1732, 1988.

Meyers, G., Annual variations in the slope of the 14°C isotherm along the equator in the Pacific Ocean, *J. Phys. Oceanog.*, *9*, 885–891, 1979.

Mix, A. C., A. E. Morey, N. G. Pisias, and S. W. Hostetler, Foraminiferal faunal estimates of paleotemperature: Circumventing the no-analog problem yields cool ice age tropics, *Paleoceanography*, *14*, 350–359, 1999.

Molina-Cruz, A., The relation of the southern trade winds of upwelling processes during the last 75,000 years, *Quat. Res.*, *8*, 324–338, 1977.

Moore Jr., T. C., et al., The reconstruction of sea surface temperatures in the Pacific Ocean of 18,000 B.P., *Mar. Micropaleontol.*, *5*, 215–247, 1980.

Murray, J. W., R. T. Barber, R. M. Roman, M. P. Bacon, and R. A. Freely, Physical and biological controls on carbon cycling in the equatorial Pacific, *Science*, *266*, 58–65, 1994.

Murray, R. W., M. Leinen, and A. R. Isern, Biogenic flux of Al to sediment in the central equatorial Pacific Ocean: Evidence for increased productivity during glacial periods, *Paleoceanography*, *8*, 651–670, 1993.

Ninnemann, U. S., and C. D. Charles, Regional differences in Quaternary Subantacrtic nutrient cycling: Link to intermediate and deep water ventilation, *Paleoceanography*, *12*, *4*, 560–567, 1997.

Pacanowski, R. C., and S. G. H. S. G. H. Philander, Parameterization of vertical mixing in numerical models of tropical oceans, *J. Phys. Oceanog.*, *11*, 1443–1451, 1981.

Patrick, A., and R. C. Thunell, Tropical Pacific sea surface temperatures and upper water column thermal structure during the Last Glacial Maximum, *Paleoceanography*, *12*, 649–657, 1997.

Paytan, A., M. Kastner, and F. P. Chavez, Glacial to interglacial fluctuations in productivity in the equatorial Pacific as indicated by marine barite, *Science*, *274*, 1355–1357, 1996.

Pedersen, T. F., Increased productivity in the eastern equatorial Pacific during the Last Glacial Maximum (19,000 to 14,000 yr B.P.), *Geology*, *11*, 16–19, 1983.

Pedersen, T. F., Timing of late Quaternary productivity pulses in the Panama Basin and implications for atmospheric CO_2, *Paleoceanography*, *6*, 657–677, 1991.

Pedersen, T. F., M. Pickering, J. S. Vogel, J. N. Southon, , and D. E. Nelson, The reponse of benthic foraminifera to productivity cycles in the equatorial Pacific: Faunal and geochemical constraints on glacial bottom water oxygen levels, *Paleoceanography*, *3*, 157–168, 1988.

Peltier, W. R., Mantle viscosity and ice-age ice sheet topography, *273, 5280*, 1359–1364, 1996.

Philander, S. G. H., and Y. Chao, On the contrast between the seasonal cycles of the equatorial Atlantic and Pacific Oceans, *J. Phys. Oceanog.*, *21*, 1399–1406, 1991.

Philander, S. G. H., and P. Delecluse, Coastal currents in low latitudes (with application to the Somali and El Niño Currents), *Deep Sea Res. Part I*, *30*, 887–902, 1983.

Philander, S. G. H., and R. C. Pacanowski, The generation of equatorial currents, *J. Geophys. Res.*, *85*, 1123–1136, 1980.

Philander, S. G. H., and R. C. Pacanowski, Response of

equatorial oceans to periodic forcing, *J. Geophys. Res.*, *86*, 19031–19061, 1981.

Philander, S. G. H., and R. C. Pacanowski, The mass and heat budget in a model of the tropical Atlantic Ocean, *J. Geophys. Res.*, *91*, 14,212–14,220, 1986a.

Philander, S. G. H., and R. C. Pacanowski, A model of the seasonal cycle in the tropical Atlantic Ocean, *J. Geophys. Res.*, *91*, 14,192–14,206, 1986b.

Philander, S. G. H., W. J. Hurlin, and A. D. Seigel, Simulation of the seasonal cycle of the tropical Pacific Ocean, *J. Phys. Oceanog.*, *17*, 1986–2002, 1987.

Pisias, N. G., and A. C. Mix, Spatial and temporal oceanographic variability of the eastern Equatorial Pacific during the late Pleistocene: Evidence from Radiolaria microfossils, *Paleoceanography*, *12*, 381–393, 1997.

Pisias, N. G., and D. K. Rea, Late Pleistocene paleoclimatology of the central equatorial Pacific: Sea surface response to the southeast trade winds, *Paleoceanography*, *3*, 21–37, 1988.

Prell, W., The Stability of low-latitude sea surface temperatures: An evaluation of the CLIMAP reconstruction with emphasis on the positive SST anomalies, *Tech. Rep., TR 025*, 60 pp. U. S. Dep. of Energy, Washington, D. C., 1985.

Ravelo, A. C., and N. J. Shackleton, Evidence for surface-water circulation changes at Site 851 in the eastern tropical Pacific Ocean, *Proc. Ocean Drill. Program, Sci. Res.*, edited by N. G. Pisias et al., vol. 138, 503–514, 1995.

Ravelo, A. C., R. G. Fairbanks, and S. G. H. Philander, Reconstructing tropical Atlantic hydrography using planktonic foraminifera and an ocean model, *Paleoceanography*, *5, 3*, 409–431, 1990.

Rea, D. K., Aspects of atmospheric circulation: The late Pleistocene (0-950,00 yr) record of eolean deposition in the Pacific Ocean, *Palaeogeog. Palaeoclimatol. Palaeoecol.*, *78*, 217–227, 1990.

Rea, D. K., L. W. Chambers, J. M. Chuey, T. R. Janacek, M. Leinen, and N. G. Pisias, A 420,000-year record of cyclicity in oceanic and atmospheric processes from the eastern Equatorial Pacific, *Paleoceanography*, *1*, 577–586, 1986.

Rea, D. K., N. G. Pisias, and T. Newberry, Late Pleistocene paleoclimatology of the central equatorial Pacific: Flux patterns of biogenic sediments, *Paleoceanography*, *6*, 227–244, 1991.

Richardson, P. L., and S. G. H. Philander, The seasonal variations of surface currents in the tropical Atlantic Ocean: A comparison of ship wind drift data with results from a general circulation model, *J. Geophys. Res.*, *92*, 715–724, 1987.

Rind, D., and D. Peteet, Terrestrial conditions at the last glacial maximum and climap sea-surface temperature estimates; are they consistent?, *Quat. Res.*, *24*, 1–22, 1985.

Romine, K., Late quaternary history of atmospheric and oceanic circulation in the eastern equatorial Pacific, *Mar. Micropaleontol.*, 7, 163–187, 1982.

Rosati, A., and K. Miyakoda, A general circulation model for upper ocean simulation, *J. Phys. Oceanog.*, *18*, 1601–1626, 1988.

Rosell-Melé, A., K.-C. Emeis, P. Farrimond, J. Grimalt, P. J. Müller, and R. R. Schnieder, Project takes a new look at past sea surface temperatures, *Eos Trans. AGU*, *79*, 393–394, 1998.

Sanyal, A., N. G. Hemming, W. S. Broecker, and G. N. Hanson, Changes in pH in the eastern equatorial Pacific across stage 5-6 boundary based on boron isotopes in foraminifera, *Global Biogeochem. Cycles*, *11*, 125–133, 1997.

Sarnthein, M., K. Winn, J. C. Duplessy, and M. R. Fontugne, Global variations of surface ocean productivity in low and mid latitudes; influence on CO_2 reservoirs of the deep ocean and atmosphere during the last 21,000 years, *Paleoceanography*, *3*, 361–399, 1988.

Shackleton, N. J., M. A. Hall, J. Line, and C. Shuzi, Carbon isotope data in core V19-30 confirm reduced carbon dioxide concentrations in the ice age atmosphere, *Nature*, *306*, 319–322, 1983.

Slutz, R. J., S. J. Lubker, J. D. Hixcox, S. D. Woodruff, R. L. Jenne, D. H. Joseph, P. M. Steurer, and J. D. Elms, *Comprehensive Ocean-Atmosphere Data Set: Release 1*, Environ. Res. Lab, Clim. Res. Prog., Boulder, Colo., (Available as *PB86-105723* from Natl. Tech. Inf. Serv., Springfield, Va.), 1985.

Tans, P. P., I. Y. Fung, and T. Takahashi, Observational constraints on the global atmospheric CO_2, *Science*, *247*, 1431–1438, 1990.

Thunell, R., D. Anderson, D. Gellar, and Q. M. Miao, Sea-surface temperature estimates for the tropical western Pacific during the last glaciation and their implications for the Pacific warm pool, *Quat. Res.*, *41*, 255–264, 1994.

Toggweiler, J. R., and S. Carson, What are upwelling systems contributing to the ocean's carbon and nutrient budgets?, *Upwelling in the Ocean: Modern Processes and Ancient Records*, edited by C. P. Summerhayes et al., p. 337–360, John Wiley and Sons. Ltd., New York, 1995.

Toggweiler, J. R., K. Dixon, and W. S. Broecker, The Peru upwelling and the ventilation of the South Pacific thermocline, *J. Geophys. Res.*, *96*, 20,467–20,497, 1991.

Wacongne, S., Dynamical regimes of a fully nonlinear stratified ocean model of the Atlantic equatorial undercurrent, *J. Geophys. Res.*, *94*, 4801–4815, 1989.

Wacongne, S., On the difference in strength between Atlantic and Pacific undercurrents, *J. Phys. Oceanog.*, *20*, 792–799, 1990.

Watkins, J. M., A. C. Mix, and J. Wilson, Living planktic foraminifera: Tracers of circulation and productivity regimes in the central equatorial Pacific, *Deep Sea Res. Part II*, *43*, 1257–1282, 1996.

Woodruff, S. D., R. J. Slutz, R. J. Jenne, and P. M. Steurer, A comprehensive ocean-atmosphere data set, *Bull. Am. Meteorol. Soc.*, *68*, 1239–1250, 1987.

Wyrtki, K., The horizontal and verical field of motion in the Peru current, *Bull. Scripps Inst. Oceanogr.*, *8*, 313–346, 1963.

Wyrtki, K., Oceanography of the eastern equatorial Pacific Ocean, *Oceanogr. Mar. Biol. Annu. Rev.*, *4*, 33–68, 1966.

Wyrtki, K., An estimate of equatorial upwelling in the Pacific, *J. Phys. Oceanog.*, *11*, 1205–1214, 1981.

Wyrtki, K., and B. Kilonsky, Mean water and current structure during the Hawaii-to-Tahiti experiment, *J. Phys. Oceanog.*, *14*, 242–265, 1984.

Yu, Z., P. S. Schopf, and J. P. McCreary, On the annual cycle of upper-ocean circulation in the eastern equatorial Pacific, *J. Phys. Oceanog.*, *27*, 309–324, 1997.

D. H. Andreasen, Earth Sciences Department, University of California 1164 High Street, Santa Cruz, CA 95064. (andreasn@aphrodite.ucsc.edu)

A. J. Broccoli, Geophysical Fluid Dynamics Laboratory, Princeton University, P.O. Box 308, Princeton, NJ 08544.

A. C. Ravelo, Institute of Marine Sciences, University of California, Santa Cruz, CA 95064. (acr@aphrodite.ucsc.edu)

(Received October 5, 1999; revised August 1, 2000; accepted September 13, 2000.)